Inferrence of effective river properties from remotely sensed observations of water surface

Pierre-André Garambois, Jerome Monnier

Inference of effective river properties from remotely sensed observations of water surface

Pierre-André Garambois and Jérôme Monnier

April 13, 2015

p.garambois@gmail.com

Abstract

The future SWOT mission (Surface Water and Ocean Topography) will provide cartographic measurements of inland water surfaces (elevation, widths and slope) at an unprecedented spatial and temporal resolution. Given synthetic SWOT like data, forward flow models of hierarchical-complexity are revisited and few inverse formulations are derived and assessed for retrieving the river low flow bathymetry, roughness and discharge (A_0, K, Q). The concept of an effective low flow bathymetry A_0 (the real one being never observed) and roughness K, hence an effective river dynamics description, is introduced. The few inverse models elaborated for inferring (A_0, K, Q) are analyzed in two contexts: 1) only remotely sensed observations of the water surface (surface elevation, width and slope) are available ; 2) one additional water depth measurement (or estimate) is available. The inverse models elaborated are independent of data acquisition dynamics; they are assessed on 91 synthetic test cases sampling a wide range of steady-state river flows (the Froude number varying between 0.05 and 0.5 for 1 km reaches) and in the case of a flood on the Garonne River (France) characterized by large spatio-temporal variabilities. It is demonstrated that the most complete shallow-water like model allowing to separate the roughness and bathymetry terms is the so-called low Froude model. In Case 1), the resulting RMSE on infered discharges are on the order of 15% for first guess errors larger than 50%. An important feature of the present inverse methods is the fairly good accuracy of the discharge Q obtained, while the identified roughness coefficient K includes the measurement errors and the misfit of physics between the real flow and the hypothesis on which the inverse models rely; the later neglecting the unobserved temporal variations of the flow and the inertia effects. A compensation phenomena between the indentified values of K and the unobserved bathymetry A_0 is highlighted, while the present inverse models lead to an effective river dynamics model that is accurate in the range of the discharge variability observed. In Case 2), the effective bathymetry profile for 80 km of the Garonne River is retrieved with 1% relative error only. Next, accurate effective topography-friction pairs and also discharge can be inferred. Finally, defining river reaches from the observation grid tends to average the river properties in each reach, hence tends to smooth the hydraulic variability.

Keywords: River hydraulics, inverse problem, effective bathymetry, bathymetry, discharge, SWOT, equifinality.

1 Context of the issue

The spatial and temporal distribution of continental water fluxes including stream and rivers is still roughly known which currently limits our representation of the water cycle and also an integrated and sustainable water management. However, current remote sensing techniques led to interesting results, such as the gravity field of water storage change via GRACE (Han et al. (2005); Munier et al. (2012)), surface water elevations via

altimetry (Frappart et al. (2006)), or radar measurements from the Shuttle Radar Topography Mission (Jung et al. (2010)). The future Surface Water and Ocean Topography (SWOT) mission with a swath mapping radar interferometer would provide new measurements of inland water surface elevation (WSE) for rivers, wetlands and reservoirs. Maps of water elevations are expected at a resolution of $100m$ with a centimetric vertical accuracy when averaged over $1km^2$ (Rodriguez (2012)). But the highlight of SWOT will be its almost global coverage and temporal revisits on the order of 1 to 4 times per $22-days$ repeat cycle. These data will offer possibilities to better characterize the spatial and temporal variabilities of inland water surfaces (e.g. Biancamaria et al. (2010)).

Estimating river discharge is not straightforward. As a good quality rating curve is needed to estimate discharge accurately from in-situ water depth records, adequate methods are required to exploit the informative content of remotely sensed hydraulic information. Based on hydraulic geometry relationships, general statistical relationships between air-space borne observations of river characteristics and discharge were developed from Gauckler–Manning–Strickler equation by Bjerklie et al. (2003, 2005) on a large sample of rivers. Note that all of those methods also rely on data about the depth and/or cross-sectional velocity profiles. Recently, Birkinshaw et al. (2014) use the equations from Bjerklie et al. (2003), water depth estimated from altimetric data ERS-2 and ENVISAT and water surface width from Landsat imagery to estimate discharge on the Mekong River. Statistical approaches based on remotely sensed observations of rivers are pertinent; nevertheless satellite measurements such as SWOT ones will not provide information about the key parameters that river bathymetry and roughness are and equifinality problems exist (e.g. Aronica et al. (1998)). Generally, the determination of the parameters embedded in open channel flow equations is not straightforward and it is still an opened and active research topic. Several studies tested the feasibility of identifying bathymetry and/or discharge with various density of observations, unknown parameters, model complexity and inverse methods.

Roux and Dartus (2005); Roux (2004) on synthetic test cases show the potential of water surface width observation to characterize flood hydrograph, with an a priori bathymetry. Roux and Dartus (2006) estimated a synthetic flood hydrograph ($Nash \sim 0.9$) by minimizing the distance between 1D shallow-water (SW) model outputs and flood extents observations rather dense in time, assuming the channel geometry and flow resistance variables are known. Based on 2D SW models, variational methods allowing state variables and/or model parameters identification are proposed in Bélanger and Vincent (2005); Honnorat et al. (2006); Honnorat (2007). For example, this method is tested on the Pearl River (China) where upstream and downstream boundary conditions on water levels can be identified with water levels measured at gauge stations, Honnorat et al. (2006); the river bathymetry and roughness are supposed to be known. Lai and Monnier (2009) estimate the inflow discharge and the roughness for synthetic 2D flood plain flows and the use of different densities of spatially distributed water level observations (snapshot of the flood plain). The inverse mathematical model is based on the 2D SW equations and variational data assimilation combining the partial snapshot images and partial time series of water levels at one gauge station. This variational data assimilation framework is applied to the Moselle River in the case of a flood event Hostache et al. (2010). Also, it is demonstrated in Hostache et al. (2010) that the amount of hydraulic information contained in partial in-situ water depth observations and the flood plain SAR image may be insufficient to identify the inflow discharge.

An essential question is the estimation of the bathymetry for the main channel of rivers which is hardly measurable from space or airborne. Durand et al. (2010) estimate the bathymetry and discharge of the Ohio river (mean $RMSE \sim 10.9\%$ over one year) through an optimization in the least square sense based on Gauckler–Manning–Strickler's equation with synthetic SWOT measurements. The estimate is based on the conservation of discharge between two reaches and is applicable only if slope variability is significant between two reaches; the river roughness is supposed to be known. Biancamaria et al. (2011) improve the estimation of the bathymetry and discharge of an Arctic river through the assimilation of synthetic SWOT observations, assuming that river bathymetry and roughness are known. In Gessese et al. (2011); Gessese (2013) basic bathymetries (eg a single smooth bump) are identified from extremely dense measurements of water levels by inverting an explicit time-step scheme, while the roughness is supposed to be known. For the same kind of bathymetries, an analytical expression of the bathymetry is proposed in Gessese et al. (2013) in the case of one in-situ observation. This original analytical approach is revisited and re-analyzed in the present study.

Yoon et al. (2012) use a 1D simplified SW model forced with input discharges from a rainfall runoff model. They assimilate synthetic observations corresponding to 8 22-days cycles of SWOT with an ensemble Kalman filter. The discharge estimation over the Ohio river basin is improved (mean $RMSE \sim 10.5\%$). They assume the cross section is rectangular and the roughness coefficient are known a priori. Honnorat et al. (2009) demonstrate the feasibility of identifying bathymetry, roughness, surface velocity - mean velocity ratio and inflow discharge in a channel by assimilating particle trajectories at the water surface (Lagrangian data); one of the interesting point is the effective bathymetry highlighted, here in the case of a 3D flow over a weir "viewed" by a 2D shallow water model (Honnorat et al. (2010)).

From real inundation extent observations, Roux and Dartus (2008) with a probabilistic method and uncertainty analysis (GSA-GLUE), identify parameters sets composed of river roughness, bathymetry and downstream discharge. Plausible parameters sets are those producing the best likelihoods values when comparing simulated (with 1D permanent SW equations) and observed flow top width. This method is tested for flood events on a 1.5 km reach of a small river; parameter ranges must be defined a priori. Negrel et al. (2011) propose a method for large rivers based on Gauckler–Manning–Strickler equation and on the depth averaged velocity profile. This profile is derived from water surface velocities estimations hence somehow imposing the roughness coefficient. The surface velocities are obtained from SAR measurements (e.g. Romeiser et al. (2007)), or more recently from MODIS data with in situ calibration (Tarpanelli et al. (2013)). Given SWOT observables, i.e. river surface elevation, width and slope, Durand et al. (2014) propose an inference based on reach averaged Gauckler–Manning–Strickler equation and mass conservation integrated in time between river snapshots. The latter integration introduces a scaling between the data acquisition interval and the roughness coefficient as it is shown in the present study. Then, a Bayesian MCMC method is used to compute a posteriori distribution functions (requiring an hypothesis on the prior distribution function). The algorithm is tested with three twin experiments for one in bank and one out-of-bank flood events on the Severn river in the UK, for three reaches of about 7 km. The sensitivity of the results to the first guess choice is not be investigated.

In the present paper, the identifiability of flow controls as a triplet $(K, b, Q(t))$ formed by river roughness, bathymetry and discharge from SWOT like measurements is investigated into details; resolutions are performed with simple and well controlled inverse methods. The identification of river properties from remotely sensed observations involves a trade-off between inverse model complexity and data informative content, density and accuracy. Somehow, the question examined in the present paper can be formulated as follows: in the SWOT context, which models (direct and inverse) complexity is adapted for retrieving the (bathymetry, roughness) pair, or effective ones, and finally the discharge ? This question is of paramount importance to elaborate reliable river dynamic models. First the forward models are re-derived following a decreasing complexity flow equations in the SWOT context, starting from the classical 1D Saint-Venant equations; next the corresponding inverse model formulations are addressed. The river sections/reaches are defined from the observation grid that is given (e.g. 1 km reach length). It is shown that the most complete physical model which allows to separate the bathymetry from the roughness coefficient is the low Froude model (the so called zero inertia SW in Gessese et al. (2013)). The inverse models built in this study tackle the question of flow representation given the scale of observation grid. Discharge identifications are performed for various flow configurations and in SWOT context. Moreover, the reliability of the effective bathymetry infered, then the resulting (bathymetry-friction) pairs are analyzed and assessed on a large panel of synthetic river cases but also on a real test case on a flood hydrograph.

The paper is structured as follows. The forward models of decreasing complexity describing river flows in SWOT context are presented in Section 2. In Section 3, the corresponding inverse problems are investigated. The relationship between the frequency of SWOT's revisits and flow dynamics is analyzed; the question of equifinality is also addressed. Section 4 introduces the twin experiments on a large panel of rivers and a real test case (Garonne river) characterized by large spatio-temporal variabilities. The generation of SWOT like data and the methods for solving the inverse problems are detailed. Results and discussions are exposed in Section 5 both for the large panel of synthetic rivers and the Garonne river. First the inversion of the triplet is performed; a rerun of the discharge is computed given the two other identified parameters. After that the bathymetry value is retrieved from its explicit expression. An analysis of the impact of the physical misfit between the observed flow and the inverse model physical assumptions is presented along with a sensitivity

analysis to measurement errors. Sensitivity of the inverse models with respect to the first guess is assessed. An enriched model and its inversion is presented in the annex (Section 9).

2 Forward Modeling

In this section, the forward flow models and physical hypothesis made are presented. Models of decreasing physical complexity are considered in view to maximize the benefit of river surface observations within inverse approaches.

2.1 Gradually varied steady state flows

Open channel flows are commonly described with depth integrated Saint-Venant equations (see e.g.Carlier (1982); Chow (1959)). The time scale of SWOT observations prevents to observe fast temporal dynamics (cf. Section 3.1). Thus we assume permanent states of rivers at each observation time. For permanent flows, the Saint-Venant equations with no lateral inflow reduces to:

$$\partial_x Q = 0 \tag{2.1}$$

$$\partial_x \left(\frac{Q^2}{A} \right) + gA \left(\partial_x Z + J \right) = 0 \tag{2.2}$$

A is the wetted surface, i.e. the cross sectional surface occupied by the fluid $[m^2]$, Q is the discharge $[m^3.s^{-1}]$, g is the acceleration of gravity $[m.s^{-2}]$, Z is the free surface elevation $[m]$, J is the energy slope $[m.m^{-1}]$, also called linear head loss. V is the mean cross sectional velocity $[m.s^{-1}]$, x is the curvilinear abscissa $[m]$ over the domain $\mathcal{D}$ and t the time $[s]$. The linear head loss is commonly expressed with Gauckler–Manning–Strickler formula: $J = \frac{Q|Q|}{D^2} = \frac{Q|Q|}{K^2 A^2 R_h^{4/3}}$. D is the conveyance capacity of the channel, R_h is the hydraulic radius defined as the ratio between wetted surface and wetted perimeter, K is the Strickler roughness coefficient $[m^{1/3}.s^{-1}]$. For 1D models, channel geometry is represented through a succession of cross sections referenced along the channel. This kind of models gives the evolution in time of the discharge through each cross section (or the mean velocity). In this study we consider no lateral inflows.This system rewrites:

$$\partial_x Q = 0 \tag{2.3}$$

$$\partial_x h = \frac{I - J}{1 - Fr^2} \tag{2.4}$$

With h the water mean depth accounted from river bed $[m]$, $I = -\partial_x b$ is river bed slope $[m.m^{-1}]$, J is the energy slope $[m.m^{-1}]$ calculated with Gauckler–Manning–Strickler formula, Fr is the Froude number $Fr^2 = \frac{Q^2 w}{gA^3}$ with w the water surface width $[m]$. Consider a river geometry with rectangular cross sections given by $b(x)$ the river bed elevation, and $w(x)$ the water surface width. Under the hypothesis of a wide rectangular cross section such that $R_h \approx h$, we have $J = \frac{Q|Q|}{K^2 w^2 h^{10/3}}$ and $Fr^2 = \frac{Q^2}{gw^2 h^3}$

2.2 Low Froude flow model

In all the forthcoming inverse modeling approaches, an important simplified model is the so-called "Low Froude model", which basically neglects the inertia term (typically $Fr < 0.3$ leads to $(1 - Fr^2) \sim 1$ at 10% error). Under this low Froude assumption, for permanent flows, and wide rectangular cross sections such that $R_h \approx h$, the system of equations (2.3) and (2.4) reduces to:

$$\partial_x Q = 0 \tag{2.5}$$

$$\partial_x h = -\partial_x b - \frac{Q\,|Q|}{K^2 w^2 h^{10/3}} \tag{2.6}$$

The systems of equations (2.3) and (2.4) or (2.5) and (2.6) are first order differential equations in x, so one boundary condition is necessary for each variable Q and h. When the flow is sub-critical ($Fr^2 < 1$), a downstream boundary condition is needed, i.e. at the outlet of the domain. A high-order Runge-Kutta numerical scheme is a good candidate to solve accurately these systems of differential equations. Remark that the low Froude model has been used and inverted in Gessese et al. (2013) (and called the zero inertia shallow water equation).

3 Inverse modeling methods and effective bathymetry

The inverse models derived in this study aim at infering the river bathymetry, the roughness coefficient and the discharge, given SWOT like data. Based on the decreasing complexity models presented in the previous section, the investigation of different inverse models is done. Two contexts are examined for observations: case 1) only remotely sensed data of water surface elevation, width and slope are available; case 2) one extra in-situ depth measurement is available. In this section, few inverse formulations are elaborated and analyzed in these two cases, then these formulations are assessed in next section.

First, an important remark preventing to straightforwardly link the flow dynamics to the data acquisition dynamics is highlighted. Next an inverse model that aims at infering the three parameters (A_0, K, Q), namely low flow bathymetry, roughness and discharge, is elaborated and discussed in Case 1)**.** The concept of an effective bathymetry is introduced. In Case 2), it is demonstrated that the most complete physical model that allows to separate the bathymetry variable from the friction coefficient is the so-called low Froude model ($Fr^2 << 1$). Then, the corresponding explicit expression of river bathymetry, given the SWOT like river surface observation at one time and one in-situ measurement, is derived in details, with the corresponding error estimates.

Given the unobserved low flow bathymetry A_0, real or effective one, two inverse formulations leading to identify the pair (K, Q) are detailed.

In other respect, a short analysis demonstrates the potential equifinality problems encountered in the identification of (K, Q) , while different orders of magnitude are highlighted for sensitivities to inverse model unknowns.

3.1 Revisiting frequency and flow dynamics relationship

The data acquisition process is considered before deriving inversion algorithms. The conservation equations with a temporal variation of mass balance and the Gauckler–Manning–Strickler's equation applied to water surface slope for the momentum are:

$$\begin{cases} \partial_x Q + \partial_t A = 0 \\ Q = K A R_h^{2/3} \sqrt{S} \end{cases} \tag{3.1}$$

with S the local water surface slope. As stated in Section 2.1 space measurements only provide observations of rivers flow at a given time. Let us set the dimensionless time $t = T^* \bar{t}$, t is the physical time in (s) and T^*in (s) is the characteristic time scale of the flow dynamics; and $\bar{t}$ is the dimensionless time. Substituting the momentum equation into the mass equation and assuming K is constant in space, see (3.1), gives:

$$\partial_{\bar{t}} A + T^* K \partial_x \left(A R_h^{2/3} \sqrt{S} \right) = 0 \tag{3.2}$$

This equation highlights the dependency of the Strickler coefficient K to the characteristics time scale T^*. This simple remark prevents to consider the unsteady mass equation integrated over satellite overpass time

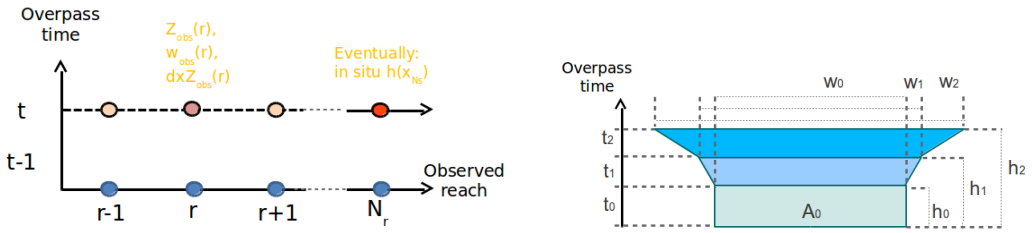

Figure 1: Inverse model discretization. (left) The spatial grid of observations is imposed by the instruments. The hydraulic sections-reaches (r) grid fits the observation grid. (right) Section view. Time overpasses are ordered by increasing flow height. The lower wetted-section A_0 is not measured.

laps; in such a case it would introduce on roughness coefficient a scaling related to the data acquisition interval**.**

3.2 Retrieving the triplet (A_0, K, Q)

SWOT observables will be spatially distributed measurements of river surface elevation Z, width w and slope S with temporal revisits. Under the assumption that the flow is permanent uniform per "sections", infering unobservable flow controls and discharge reduces to the identification of the unobservable triplet (A_0, K, Q). In this context, the inverse models to be solved are derived.

3.2.1 The basic inverse model: permanent uniform flow per section

For each reach/sections, we assume the flow is permanent and uniform; hence the equations are:

$$\begin{cases} \partial_x Q = 0 \\ Q = KAR_h^{2/3}\sqrt{S} \end{cases} \tag{3.3}$$

We assume the roughness coefficient K to be constant both in space and time. We set :

$$\phi = AR_h^{2/3}\sqrt{S} \tag{3.4}$$

As a matter of facts, the spatial discretization appears to be imposed by the observation grid, i.e. the spatial resolution of the remotely sensed observations. In discrete form, and following river discretization into reaches as showed in Figure 1, we seek to solve the following system :

$$\begin{cases} Q_{r_1,p} = ... = Q_{N_R,p} \\ Q_{r,p} = K.\phi_{r,p} = KA_{r,p}^{5/3}w_{r,p}^{-2/3}\sqrt{S_{r,p}} \end{cases} \quad \forall r \in [1..N_r], \forall p \in [1..N_p] \tag{3.5}$$

with r being the reach number and N_r the total number of reaches, p the satellite pass number and N_p the total number of satellite observation considered in time. Each reach r at observation time p, is characterized by its water surface slope $S_{r,p}$, width $w_{r,p}$ and its cross sectional wetted area $A_{r,p}$. There are several ways to write and solve this system and two of them are studied below. They will be studied on a large sample of synthetic river geometries and on the Garonne River downstream Toulouse in the next sections.

3.2.2 Trapezoidal profiles

Among all available observations of a river in time, A_0 denotes the unobserved wetted area below the lowest flow observation, see Figure 1 (right). All other observations being for higher flow conditions, the cross-sectional area of a reach is given by:

$$A_{r,p}(h) = A_{0,r} + \delta A_{r,p} = A_{0,r} + \int_{h_0}^{h_{Np}} w_r(h')dh' \tag{3.6}$$

Since the different water surface elevations and width will be observed, trapezoidal areas can be calculated between the lowest and the highest water surface elevations. Then, the δA variation is approximated using trapezoidal integration over the time series of measurements as proposed by Durand et al. (2014):

$$\int_{h_t}^{h_{t+1}} w_r(h')dh' \approx \frac{w_r(t+1) + w_r(t)}{2} \left[h(t+1) - h(t)\right] \tag{3.7}$$

and,

$$R_h = \frac{A}{Perimeter} = \frac{(A_0(r) + \delta A(r,p))}{(w_0 + 2h_0)_{(r)} + P_{obs}(r,p)} \sim (A_0(r) + \delta A(r,p)).(w^{obs})^{-1} \tag{3.8}$$

For rivers with a large width-to-depth ratio, the width is a good approximation of the wetted perimeter (see e.g. Strelkoff and Clemmens (2000)). Finally, the inverse model to be solved writes:

$$\begin{cases} Q_{1,p} = ... = Q_{N_R,p} \\ Q_{r,p} - K(A_{0,r} + \delta A_{r,p})^{5/3} w_{r,p}^{-2/3} \sqrt{S_{r,p}} = 0 \end{cases} \quad \forall r \in [1..N_R], \forall p \in [1..N_P] \tag{3.9}$$

For more than one river observation in time, $p > 1$, recall that two contexts are studied in this paper: 1) only remotely sensed observations of the water surface are available (water surface elevation, width and slope); 2) one additional water depth measurement (or estimate) is available. In case 1) the unknowns are $Q_{r,p}$, K and $A_{0,r}$ for $r \in [1..N_r]$, $p \in [1..N_p]$ and in case 2), i.e. given $A_{0,r}$ and $A_{r,p}$ for all r, p, the unknowns are $Q_{r,p}$ and K and there are in both cases $N_r \times N_p$ equations. If the discharge is supposed non constant in space (hence writing $Q_{r,p}$), then this is an under-determined system with $N_r \times (N_p + 1) + 1$ unknowns (respectively $N_r \times N_p + 1$ unknowns in case 2)). If the discharge is supposed constant in space then this is an over-determined system with $N_r + 1 + N_p$ unknowns (respectively $N_p + 1$ unknowns in case 2)). In each case the solution will be analyzed in a general least square sense in next sections. The assumption of constant Q in space might be made or not depending on the flow dynamics observed.

Remark 1: The system (3.9) is multilinear with respect to the unknowns $Q_{r,p}^{3/5}$, $K^{3/5}$ and $A_{0,r}$. For one river snapshot, i.e. one satellite observation in time, $p = 1$, and given A_0 for each reach, this system is similar to N_r encoding public-private key type equations. Thus the present inverse problem cannot be solved for one river snapshot only.

Remark 2: By substituting the second equation of system (3.9) into the first one, the constant value K simplifies, and the system reduces to N_r equality constraints between the terms $\phi_{r,p}$. Hence in such a form the roughness coefficient K cannot be infered.

Remark 3: Following Remark 2, if the inertia term is added to the momentum equation (see Equation (2.4)), it is possible to use the mass conservation between two reaches and express the roughness in function of river surface width and slope. Nevertheless, in that case the roughness also depends on $\partial_x h$, which is in practice not possible to estimate since it requires unrealistic observation accuracy of water depth (hence the knowledge of river bathymetry profile).

3.3 Retrieving the pair (K, Q) given the underlying geometry A_0

In this section, the low flow wetted areas $A_{0,r}$ are supposed to be given for each reach $r \in [1..N_r]$. These values may be estimated either from empirical relationships based on drainage areas and rainfall statistics, or from the inversion method presented in Section (3.5). In that case, for each overpass p and each reach r, the wetted cross sectional area $A_{r,p}$ is estimated given the river surface elevation and width measurements (cf. Fig. 1). The more measurements for varying flow conditions being available, the best the approximation of

reach cross-sections is. The system to be inverted can be formulated in different ways. Below are presented the two inverse formulations stated and analyzed later. For all the systems, more than one satellite pass is considered i.e. $p > 1$.

3.3.1 Formulation I: (K, Q) constant in space

The unknown roughness K is supposed constant in time and space, the unknown discharge Q_p is supposed constant in space, then (3.9) writes as an over-determined set of $N_r \times N_p$ equations with $N_p + 1$ unknowns. Unfortunately, this discrete formulation of the inverse problem leads to a severe ill-posed problem very difficult to solve. Indeed in practice, $\phi_{r,p}$ can be largely variable in space because of observation errors or misfit between inverse model physics and observed physics (inertia terms, non permanent flow and variations of mass balance). Drawing on this, the formulation that is used for flow parameters identification on a large sample of synthetic river geometries consists in taking the average of $\phi_{r,p}$ in space for each permanent state p. Then the system (3.9) writes:

$$M_1 X_1 = \begin{pmatrix} -\frac{1}{N_r}\sum_{r=r_1}^{N_r} \phi_{r,1} & 1 & 0 & \dots & 0 \\ \vdots & & & \ddots & \\ -\frac{1}{N_r}\sum_{r=r_1}^{N_r} \phi_{r,N_p} & 0 & 0 & \dots & 1 \end{pmatrix} \begin{pmatrix} K \\ Q_1 \\ \vdots \\ Q_{N_p} \end{pmatrix} = 0 \tag{3.10}$$

Hence it is an under-determined system with N_p equations and $N_p + 1$ unknowns (the components of X_1). Recall that: $\phi_{r,p} = A_{r,p}^{5/3} w_{r,p}^{-2/3} \sqrt{S_{r,p}}$. This system will be assessed on large number of synthetic river flows in next section.

Remark 4: There is a slight difference of accuracy between averaging $\phi_{r,p}$ in space or to let Q vary in space for identification and averaging Q afterwards. So the choice is made to let Q being variable in space for the identification of unsteady river flows - with spatial variations of discharge Q.

3.3.2 Formulation II: Q variable in space

Given a river snapshot, if rapidly varied flow occurs significant spatial variations of discharge can be induced even at relatively small spatial scales. It is the case on the Garonne river test case studied later (80 km of the Garonne river downstream Toulouse, about 150 m wide). So that, below, the unknown discharge Q is supposed variable in space, the unknown roughness K is still supposed constant in time and space. Then, the system (3.9) writes:

$$M_2 X_2 = \begin{pmatrix} -\phi_{1,1} & 1 & 0 & \cdots & 0 \\ \vdots & & \ddots & & \\ -\phi_{1,N_p} & & & & \\ \vdots & \vdots & & & \vdots \\ -\phi_{N_r,1} & & & & \\ \vdots & & & \ddots & \\ -\phi_{N_r,N_p} & 0 & \cdots & 0 & 1 \end{pmatrix} \begin{pmatrix} K \\ Q_{r_1,1} \\ \vdots \\ Q_{r_1,N_p} \\ \vdots Q_{N_r,1} \\ Q_{N_r,N_p} \end{pmatrix} = 0 \tag{3.11}$$

It is an under-determined system with $N_r \times N_p$ equations and $N_r \times N_p + 1$ unknowns. Recall that: $\phi_{r,p} = A_{r,p}^{5/3} w_{r,p}^{-2/3} \sqrt{S_{r,p}}$. This system will be assessed on the Garonne River in Section 5.

3.4 Equifinality problem and sensitivity w.r.t. each unknown

The present section aims at showing the potential equifinality problem in terms of roughness-geometry pairs (K, A), and also highlighting the different sensitivities **related to** each parameter **of** the inverse problem. The response surface of Gauckler–Manning–Strickler's equation in terms of discharge is examined for one

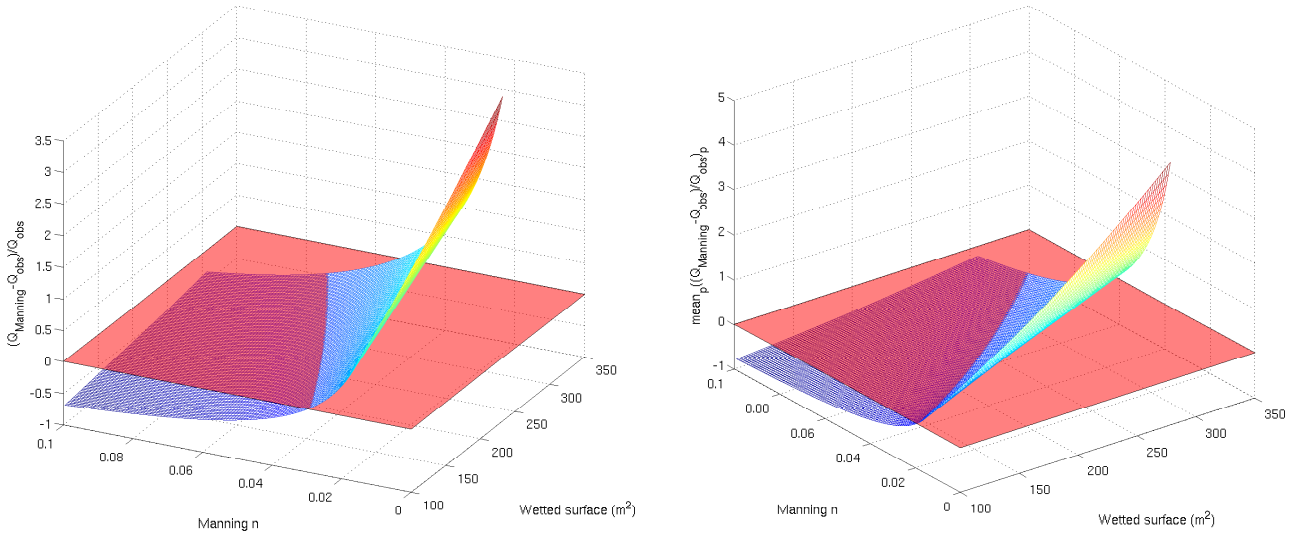

Figure 2: Forward problem, response surface of Gauckler–Manning–Strickler equation (colored surface) and best discharge estimation (transparent red plane) for (left) one and (right) three permanent states of a reach of the Garonne river test case

snapshot and three snapshots of the Garonne River, see Fig. 2. The relative error on discharge (averaged in time for the three daily discharges) is presented in figure 2, the intersection of the colored response surface with the transparent red plane represents all the pairs (K, A) producing the right value of discharge. The intersection line represents the infinity of (K, A) solutions for a given value of discharge Q. This plot illustrates the equifinality problem between roughness and geometry couples for one overpass.

Next, the sensitivity analysis of the inverse problem is examined through the normal equations of system (3.9), M_3 being the matrix of the system with the unknowns (K, Q_1, Q_2). For the sake of simplicity we consider the case $p = 2$ river observations in time and N_r reaches, the normal equations relative to the general expression for the inversion of the pair (K, Q) writes:

$$M_3^T M_3 X = \begin{pmatrix} \sum_{r,p} \phi_{r,p}^2 & -\sum_r \phi_{r,1} & -\sum_r \phi_{r,2} \\ -\sum_r \phi_{r,1} & N_r & 0 \\ -\sum_r \phi_{r,2} & 0 & N_r \end{pmatrix} \begin{pmatrix} K \\ Q_1 \\ Q_2 \end{pmatrix} \tag{3.12}$$

Let us consider the Garonne River's profile presented in Section 5. The Singular Value Decomposition defined by: $M_3^T M_3 = USV$ with unitary matrices U and V and the diagonal matrix S containing the singular values, is computed. Then, the singular value corresponding to the roughness parameter K is three orders of magnitude greater than those corresponding to the discharge values Q_1 and Q_2. This simple example illustrates the dominating sensitivities with respect to K observed in all numerical inversions performed in the present article. It also corroborates that the forthcoming error obtained on the infered K values, contains the misfit between the physical assumptions made in the inverse models and the real flow observed (plus the measurements errors).

3.5 Low Froude case and effective bathymetry identification

We have shown in Section 3.4 that the pair roughness-geometry (K, A) may be impossible to invert for one overpass only ($p = 1$). Also it will be shown in next sections that it may be difficult to invert the pair

accurately even with few overpasses. Hence, the definition of a potential model decoupling the friction term and the bathymetry may be interesting in view to invert the pair in two sequential steps. As demonstrated below, this possibility can be very interesting in practice since it leads at the end to a more accurate inversion of (A_0, K, Q) .

The idea of bathymetry identification without roughness coefficient and based on vanishing advection terms has been introduced by Gessese et al. (2013). The authors called the equations "zero-inertia" shallow water approximation (the present so-called low Froude model), and they obtained directly Equation (3.19) below, which allows to calculate explicitly the bed bathymetry from free surface elevation data. Recall that in Gessese et al. (2013), the inverse problem is solved in two spatial dimensions using the method of the characteristics. The test cases considered are basic, with very smooth geometry and very dense observations of water surface elevation. Moreover, the free surface is generated with a model that also neglects inertia terms.

In Annex 9.2, we show that the second order Equation (9.7) allows to infer iteratively the bathymetry and the friction but it would require an unrealistic accuracy on the slope data (the "initial condition" must include the depth derivative $\partial_x h$ which is not easily accesible in practice). Equation (9.7) demonstrates that the most complete model in h where the bathymetry term appears independently of the friction term, is the low Froude model, Equation (2.6).

In the present section, the bathymetry is explicitly inverted from Equation (2.6), as it has been done in Gessese (2013); in addition we derive an explicit quantification of error in function of SWOT like observation errors.

In the next sections, we use this inverse model in a SWOT data context, with real-like river data, by quantifying errors, and by analyzing numerically the method's reliability depending on the hypothesis. The later being: Fr^2 values compared to 1 and the stationary misfit of the observed flow. These analysis are performed on synthetic test cases designed to be fully representative of 1D real flows (with no lateral inflow), and real data (Garonne river).

3.5.1 Mathematical explicit inversion

The mono dimensional forward problem for wide rectangular cross sections writes:

$$\partial_x Q = 0 \tag{3.13}$$

$$\partial_x Z + \frac{Q\,|Q|}{K^2 w^2 h^{10/3}} = 0 \tag{3.14}$$

With $h(x)$ the water depth and $b(x)$ the river bed elevation, x being the spatial coordinate. And in function of the free surface elevation Z which is observable it becomes:

$$Q\,|Q| = K^2 w^2 h^{10/3} S \tag{3.15}$$

With slope $S = -\partial_x Z$ the free surface slope.

Assumption. The free surface is assumed monotonous $\partial_x Z < 0$ ans so $S > 0$, flow goes from left to right so $Q > 0$.

$$Q = K w h^{5/3} S^{1/2} \tag{3.16}$$

Deriving lubrication-like equations, the momentum equation (3.14) is substituted into the mass equation (3.13):

$$\partial_x Q = \partial_x \left(K w h^{5/3} S^{1/2} \right) = 0 \tag{3.17}$$

Under the hypothesis of a roughness coefficient K constant in space, it comes:

$$\frac{5}{3}S^{1/2}wh^{2/3}\partial_x h + wh^{5/3}\partial_x S^{1/2} + S^{1/2}h^{5/3}\partial_x w = 0 \tag{3.18}$$

So:

$$\frac{\partial_x h}{h} = -\frac{3}{5}\left(\frac{\partial_x S^{1/2}}{S^{1/2}} + \frac{\partial_x w}{w}\right) \tag{3.19}$$

by integration, the following explicit expression of h in function of the water surface slope, the width and the water depth given at one location point x_{situ} is obtained:

$$h(x) = h(x_{situ})\left(w(x_{situ})S^{1/2}(x_{situ})\right)^{3/5}\left(w(x)S^{1/2}(x)\right)^{-3/5} \tag{3.20}$$

Remark 5: An equation similar to equation (3.19) have already been derived in Gessese et al. (2013); Gessese (2013).

Remark 6: The most complete model allowing to separate the bathymetry variable from the friction one is the low Froude model. Indeed if the physical complexity of the model is increased by adding the inertia term, then the inverse model is a second order differential equation in h and one needs to approximate $\partial_x h$ accurately, which is prohibitive. Numerical experiments have been performed (not presented in this paper); they show that a spatial resolution on the order of few meters is required to ensure the convergence if solving a second order partial differential equation for bathymetry identification. This is unrealistic given the expected SWOT resolution even if measurement were error free. Several simplifications and linearizations were also tried out but all the inverse models obtained required unrealistic measurements of $\partial_x h$.

Remark 7*:* The same equation as Equation (3.19) can be derived for the hydraulic radius R_h, the water surface slope and the cross sectionnal wetted surface. In order to integrate it and find an explicit model, an a-priori hypothesis on the river cross sectionnal geometry is required.Hence justifying the current hypothesis of a rectangualr cross section.

3.5.2 Quantification of error

Since the low Froude inverse model (3.20) is an explicit formulation of $h(x)$ in function of river observables, the resulting uncertainty can be calculated explicitly too. Let us set:

$$\begin{aligned} h_{identified} &= h_{true} + \Delta h \\ w_{obs} &= w_{true} + \triangle w \\ S_{obs} &= S_{true} + \triangle S \end{aligned} \tag{3.21}$$

with $\Delta h, \triangle w, \triangle S$ being the errors on water depth, water surface width and the slope root square. Then, we get:

$$\frac{\Delta h}{h} = \frac{3}{5}\frac{\Delta w}{w} + \frac{3}{10}\frac{\Delta S}{S} \tag{3.22}$$

Remark 8: This error quantification is correct in the case of the low Froude forward model - corresponding inverse model. In others words, if observations are for river flows with higher Froude sections, the error quantification is not exact anymore. Interestingly Equation (3.22) is not a statistical but a deterministic estimation of the error that is made at least on bathymetry identification.

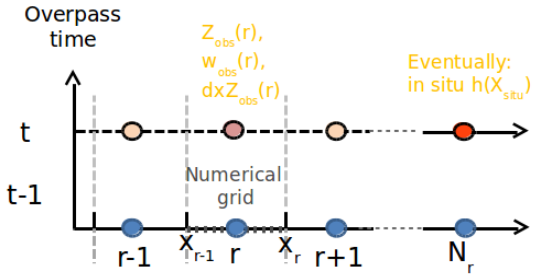

Figure 3: Forward problem grid: numerical grid within a hydraulic grid consisting in a discretization of a river into reaches (r) from SWOT observation grid. Reach boundaries defined by in-situ cross section measurements.

4 Twin experiments on a large panel of rivers

In the following the identification methods will be tested on a large number of synthetic test cases and on a real physical case (Garonne river). The observations are synthetic (twin experiments) in the sense that forward models are first performed to generate observations, next random noises are added. This twin experiments process can be detailed as follows:

- True values of the parameters to be estimated are chosen. Given these input parameters, a forward hydrodynamic model provides the flow, hence the water surface elevation, width and slope. Random noises are added to these synthetic observations to simulate the expected SWOT accuracy.
- The inverse models are performed given these data.

Let us point out that the forward model used to generate the SWOT like observations includes all the physics i.e. including the inertia term and the temporal term (unsteady model) in the case of the Garonne River.

4.1 Resolution of the forward models

A river is discretized into river reaches whose length corresponds to the resolution of observation grid, see Fig. 1. 1 km in the present study. The permanent forward problems solved are the backwater curve (Equations (2.3) and (2.4)) and the low Froude case (Equations (2.5) and (2.6)). A classical solver (Runge-Kutta 4) is used to solve these ordinary differential equations with non constant coefficients. Therefore a numerical sub-grid is used, index j (Figure 3).

4.2 Description of the large panel of synthetic rivers

First we use a synthetic test case in order to be able to investigate the influence of different parameters on the results of the identification. The bathymetry b and river width w are given at each boundary x_i of a river reach, and are assumed to vary linearly between two reach boundaries. The geometry of the synthetic river is thought to be representative of the variability that can be encountered on many real rivers. For the following test cases the Froude is roughly varying between 0.05 and 0.5 for 1 km reaches and permanent flows - note that few classifications in terms of Froude numbers have been found in the literature ; for fish habitat description Jowett (1993) propose $Fr = 0.18$ as the limit between pools and rifles. The Froude range chosen here (between 0.05 and 0.5) corresponds to a wide range of rivers from those located in foothill (mean slope$\sim$ 1/1000) to lowland rivers that are generally more flat (mean slope$\sim$ 1/10000) - for a given scale of observation of 1 km for this study in a SWOT like context. The number and the repartition of control sections is also widely sampled. For synthetic rivers the bathymetry is generated with the following equation:

	t_1	t_2	t_3
Q^t	200	400	700
$h(x_{situ})$	2.5	3.5	4.5
$min_x Fr$	0.05	0.07	0.09
$max_x Fr$	0.36	0.38	0.41
$mean_x Fr$	0.17	0.19	0.21

Table 1: Flow features of the synthetic river test case, Froude numbers of the backwater curve.

$$b(x) = (L - x)\, tan(I_0) + a_0 sin\left(\frac{2\pi \triangle x}{p_0} x\right) + a_1 sin\left(\frac{2\pi \triangle x}{p_1} x + \frac{\pi}{6}\right) \tag{4.1}$$

$\triangle x$ is the constant river reach size in this test case, L is the river length, I_0 is a constant river slope, a_0 and a_1 (resp. p_0 and p_1) are the first and second order amplitudes of bathymetry variations (resp. spatial periods) along the flow distance x. The channel cross section is supposed rectangular and constant in time, the variations in space of channel width are given by:

$$w(x) = w_0 + a_2 sin\left(\frac{2\pi \triangle x}{p_2} x\right) \tag{4.2}$$

w_0 is a constant channel width and a_2 (resp. p_2) is the first order amplitude of river width variations (resp. spatial period) along the flow distance x. The following values are chosen to produce a generic bathymetry: $L = 12$ km, $I_0 = 1.10^{-3}$, $w_0 = 100$ m, $a_0 = 1.5$ m, $a_1 = 1$ m, $a_2 = 20$ m, $p_0 = 6$ km, $p_1 = 3$ km and $p_2 = 4$ km. Note that the two modes of the bathymetry are shifted in phase with the term $\frac{\pi}{6}$ in equation (4.1). The spatial period of width variations is not a multiple of bathymetry periods. The bathymetry resulting from those choices presents a maximal local slope of $2.4.10^{-3}$. The low Froude (Equation 2.6) and backwater curve (Equation 2.4) forward models are performed, as explained in Section 4.1 and Figure 3, for three permanent states with the boundary conditions and the resulting Froude numbers given in Table 4.2. A constant roughness $K = 20\ m^{1/3}.s^{-1}$ is used.

Identifications are performed for 90 other channel geometries obtained by randomly sampling p_0, p_1 and p_2 (between 2 km and 8 km) defining the positions of control sections and a_0, a_1 (between 0 and 1.5 m) and a_2 (between 0 and 70m) defining their shapes; 30 channel geometries (cross sections repartitions and shapes) being generated for each mean slope $I_0 = 1/1000$, $I_0 = 0.5/1000$ and $I_0 = 0.1/1000$.

4.3 The Garonne river (portion downstream Toulouse)

The Garonne River drains an area of about 55000 km² in France from its headwaters in the Spanish Pyrenees near the Pic d'Aneto to the Gironde estuary, where the mouths of the Garonne and the Dordogne merge. The study zone selected is a 82 km portion of the Garonne river downstream of Toulouse (5) with a drainage area of about 10000 km²; the flow regime is rather contrasted from very low flow on the order of 50 $m^3.s^{-1}$ in summer to large peak flows: five year flood flow is 2000 $m^3.s^{-1}$. This river reach is studied in Simeoni-Sauvage (1999)and in Larnier (2010). An unsteady 1D shallow water hydraulic model is calibrated between Toulouse and Malause Larnier (2010), and the water levels will be used as a reference in the following. River morphology is described with 163 cross sections (from Simeoni-Sauvage (1999)) distant of 50 to 600m. The river is rather steep with a mean slope about 0.9×10^{-3} and its morphology characterized by a quick succession of rifles and pools. Moreover this river that is about 150m wide would represent the lower limit of SWOT detection capacity.

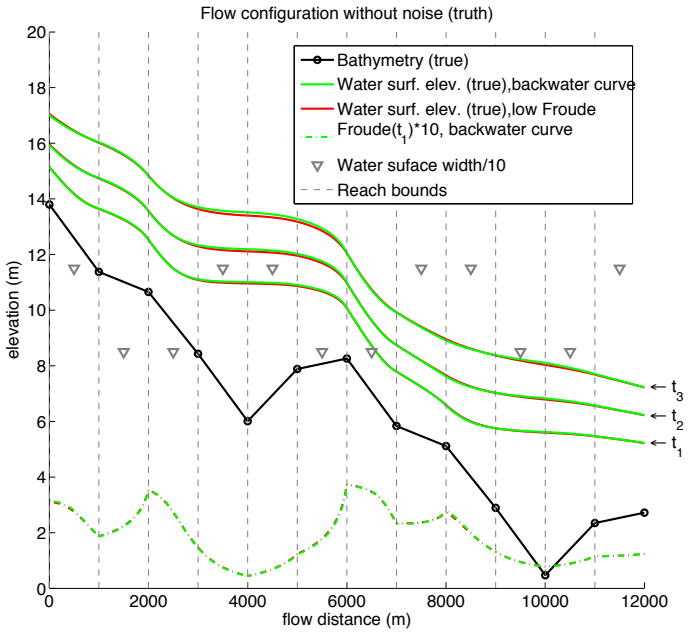

Figure 4: forward models on generic river test case configuration: permanent flows at three times without noise. Dashed lines correspond to Froude variability at t_1.

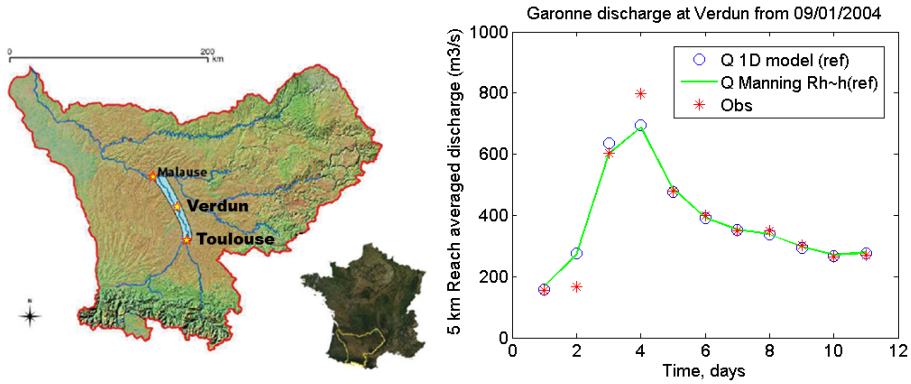

Figure 5: (left) The Garonne River study area between Toulouse-Malause, and the location of the validation gauge of Verdun sur Garonne. (Right) Comparison of observed discharge at Verdun sur Garonne with reach averaged Manning equation and 1D reference SW model for the period of interest.

Noise level	1	2	3	4	5	6	7
σ_S in $cm.km^{-1}$	0.25	0.35	0.55	0.75	0.95	1.15	1.25
σ_Z in cm	5	7	10	15	20	30	40
σ_w in m	5	7	10	15	20	30	40

Table 2: Noise levels defined for SWOT-like observables

The low Froude (Equation 2.6) and backwater curve (Equation 2.4) forward models are run following the experimental design described in section 4.1 and Figure 3. The computations are made on reaches of about 1 km defined from 1D model data with an effective bathymetry. The effective bathymetry conserves the cross sectional wetted area and the discharge from 1D model on real cross sections but its shape is as described in figure (1). The boundary conditions from the 1D model are the water levels at the downstream boundary of the whole domain and the discharges from 1D model (not accounting for lateral inflows) at the downstream boundary of each reach. Indeed the discharge is varying in space for 82 km of a real river, especially when a flood wave is propagating.

4.4 Generation of SWOT like data

In the context of twin experiments the backwater curve is used as forward model (Equation 2.4) in order to generate "true" water surfaces. for each river reach r we have w_{true}, Z_{true} and $\partial_x Z_{true}$. Note that the water surface slope is calculated from water surface elevation with a first order centered finite difference scheme on the numerical grid: $S_{true} = -\partial_x Z_{true}|_r = -\frac{Z_{r+\Delta j} - Z_{r-\Delta j}}{x_{r+\Delta j} - x_{r-\Delta j}}$ for $i \in [1 \cdots N_s]$, N_s being the number of river sections, Δj being the regular cell-size of the numerical grid (at least for each river reach r). Synthetic SWOT-like observations are then obtained by adding Gaussian noise to those quantities for a given observation time:

$$\begin{cases} w_{obs} = w_{true} + N(0, \sigma_w) \\ Z_{obs} = Z_{true} + N(0, \sigma_Z) \\ S_{obs} = S_{true} + N_i(0, \sigma_S) \end{cases} \tag{4.3}$$

Typically, the measurements errors expected from SWOT on water surface elevation, slope and width should be (Rodriguez (2012)): $\sigma_Z = 0.05m$, $\sigma_S = 0.75 \times 10^{-5}$ and $\sigma_w = 0.15w$ (this is at least what is expected for the narrowest rivers seen by SWOT) for pixel of 1 km², indeed the intrinsic resolution is less precise. The sensitivity of the identifications to measurement errors will be tested in the following. Noise is added to the "true state" of the system with a Gaussian noise (Equation 4.3). The accuracy of observations varies in function of the standard deviation σ, also called noise level. Different noise levels chosen in relatively wide ranges will be tested to generate observations (Table 2). For each noise level 100 sets of observations are generated and used as inverse model inputs in order to obtain an averaged behavior (averaged after all simulations and inversions). When different noise levels are simulated on one of the three water surface characteristics, the two others are set to measurement errors expected from SWOT.

4.5 Resolution of the inverse models

The spatio-temporal configuration of the inverse problems are presented in Figure 1. They are tested on the large panel of synthetic rivers and on the Garonne river. SWOT-like observations are generated as exposed above: water surface elevation Z, width w, and slope S. The different inverse methods tested are the following:

Method 1a: Identification of the triplet (A_0, K, Q) in the least square sense with a trust-region-reflective algorithm (e.g. Moré and Sorensen (1983)) used for solving the system (3.9) when it is over-determined, for instance when the discharge Q is searched as constant in space. Research intervals and first guess on the solution are required. Results are presented in Section 5.1.

Method 1b: Identification of the triplet (A_0, K, Q) in the least square sense when it is under-determined, i.e. when the discharge Q is searched as non constant in space. A Levenberg-Marquardt solver (e.g. Moré (1977)) is used when it is an under-determined system, i.e. when the discharge Q is searched as variable in space. Then a first guess on the solution is required. Results are presented in Section 5.4.3.

Method 2: Identification of an effective bathymetry using equation (3.20) and one in-situ water depth measurement at the location x_{situ}, such as : $h(r) = h_{obs}(x_{situ}) \left(w_{obs}(x_{situ}) S_{obs}^{1/2}(x_{situ}) \right)^{3/5} \left(w_{obs}(r) S_{obs}^{1/2}(r) \right)^{-3/5}$ for each reach r. Results are presented in Section 5.2 and 5.4.1.

Method 3: Identification of the pair (K, Q) assuming A_0 is known (from the identification using equation (3.20) and one in-situ water depth measurement). A Levenberg-Marquardt solver is used for solving the system (3.10) or (3.11), in the linearized least square sense. A first guess on the solution is required. Results are presented in Section 5.3 and 5.4.2.

Remark 9: The inverse model proposed in this study, solved in different ways depending on the observations available and/or the flow dynamics, do not depend on the data acquisition dynamics as pointed out in Section 3.1. In other words the system of equations (3.9) can be written for unevenly spaced time series of observations.

5 Results and discussions

This study focuses on the estimation of the three flow variables (A_0, K, Q) using SWOT like measurements. For that purpose, we use the inversion methods presented previously; thus highlighting their capabilities. Different tests, with different goals are presented both on a large panel of synthetic rivers and on the Garonne River.

5.1 Synthetic Rivers - Inversion of the triplet (A_0, K, Q) with method 1a

In this section the aim is to test the inversion of the triplet (A_0, K, Q) directly from equation 3.9. In order to do so, 3 SWOT like observations are used on the synthetic test case presented in Section 4.2**.** The bathymetry is plotted in Figure 4 with the three flow lines considered to generate the observations.

5.1.1 Inversion of the triplet (A_0, K, Q)

A sample of $N_{samp} = 100$ sets of random Gaussian numbers is used as SWOT like measurements of water surface, i.e. water surface elevation, width and slope as exposed in Section 4.4. For this synthetic river test case the method 1a exposed in § 4.5 is used for the identification of the triplet (A_0, K, Q). The research intervals chosen for the resolution are $[50 \dots 500]\ m^2$ and $A_0^b = 300\ m^2$ for A_0, $[1 \dots 90]\ m^{1/3}.s^{-1}$, $[180 \dots 1000] m^3.s^{-1}$for discharge. First guess values are $(K_b, Q_b^1, Q_b^2, Q_b^3) = (50, 500, 500, 500)$, while the true values are $(K_t, Q_t^1, Q_t^2, Q_t^3) = (20, 200, 400, 700)$; hence first guess RMSE on low flow bathymetry is 40%, it is 50% on discharge and 150% on roughness. The results of identification are then averaged over a significant noisy sample (Figure 6). For the identification of the triplet the A_0 RMSE is less than 3%, the error on roughness K is about 1% with $K = 20.1\ m^{1/3}.s^{-1}$ the truth being $K_t = 20\ m^{1/3}.s^{-1}$, and the discharge RMSE is 4.9% under our hypothesis. This solution is optimal in the least square sense on the N_r reaches and N_p river snapshots with a Q variable in time but with low flow cross sectional area A_0 and roughness K that are intrinsic to the range of flow regimes. This identification was also performed on the other synthetic geometries and similar performances are obtained.

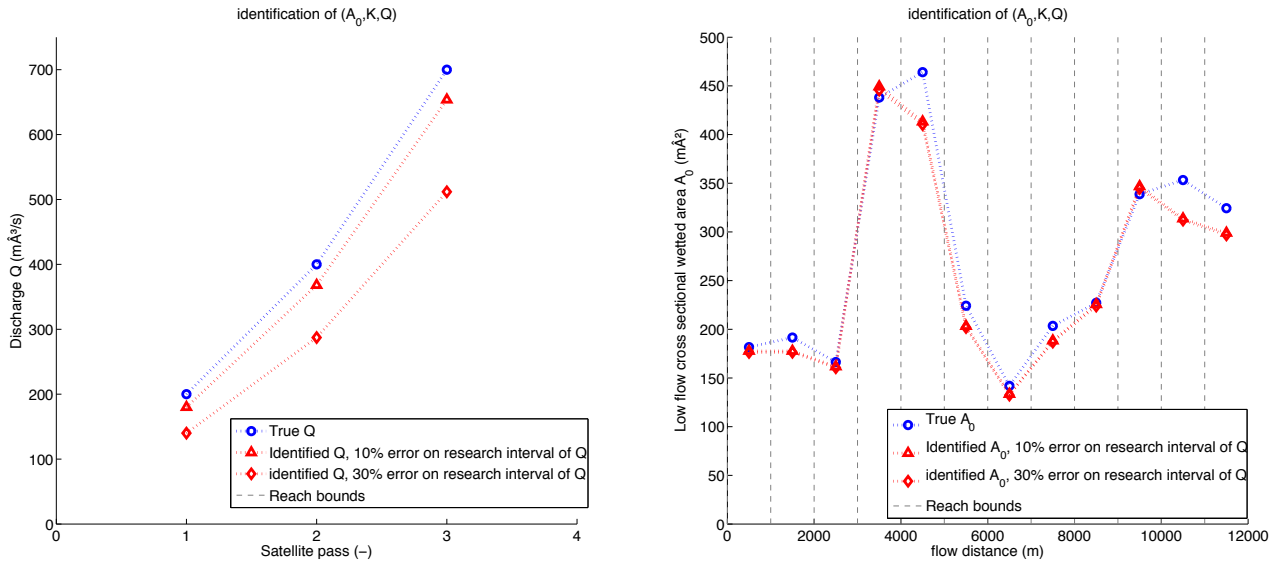

Figure 6: Results obtained while identifying the triplet (A_0, K, Q) : (left) the discharge Q, (right) the base-flow cross sectional area A_0, and the roughness $K = 20.1\ m^{1/3}.s^{-1}$ (the truth being $K_t = 20\ m^{1/3}.s^{-1}$). Observations with SWOT like errors. Flow features are summed up in Table 4.2 and Figure 4.

Research interval for Q en $m^3.s^{-1}$ with method 1a	$[180 \dots 1000]$	$[140 \dots 1000]$	$[100 \dots 1000]$
Err_{A_0}	2.7%	2.7%	2.7%
K and Err_K	20.1 and 1.1%	15.6 and 22.1%	11 and 45%
Err_Q	4.9%	17%	30.1%

Table 3: Sensitivity of the identification of the triplet (A_0, K, Q) to the research interval for discharge given SWOT-like errors. The three true values of discharges Q^t sought are $(200, 400, 700) m^3.s^{-1}$ respectively.

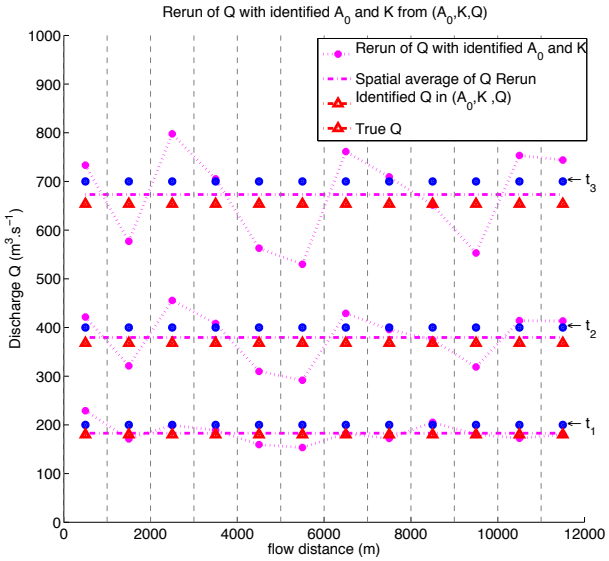

Figure 7: Re-computation of the discharge Q given A_0 and K identified at 2.7% and 1.1% relative errors (using the triplet inversion method with observations SWOT like errors amplitudes).

5.1.2 Rerun of Q based on the identified variables (A_0, K)

The goal here is to analyze the spatial and temporal errors obtained while re-computing the discharge using the identified triplet (A_0, K, Q), and still assuming that A_0 and K are constant in time. Figure 7 shows the spatial variation of Q re-computed from the identified $A_{0,r}$ and K values. The average RMSE obtained is the same than before but it can be noticed that the error is not constant in space as the identification error on $A_{0,r}$. The error budget of the momentum equation (3.3) is $\left(\frac{\sigma_Q}{Q}\right)^2 = \left(\frac{\sigma_K}{K}\right)^2 + \left(\frac{5}{3}\frac{\sigma_{A_0}}{A_0+\delta A}\right)^2 + \left(\frac{5}{3}\frac{\sigma_{\delta A}}{A_0+\delta A}\right)^2 + \left(\frac{2}{3}\frac{\sigma_w}{w}\right)^2 + \left(\frac{1}{2}\frac{\sigma_S}{S}\right)^2$, with σ_Q , σ_K, σ_{A_0}, $\sigma_{\delta A}$, σ_w, σ_S respectively being the errors on discharge, roughness, low flow cross sectional area, cross sectional area variation, river top width and water surface slope. For this re-computation, the amount of error due to the identified parameters A_0 and K is $\sqrt{\left(\frac{\sigma_K}{K}\right)^2 + \left(\frac{5}{3}\frac{\sigma_{A_0}}{A_0+\delta A}\right)^2}$. The later is equal to 4.6%, the remaining 0.3% being due to observation errors. This error on A_0 and K can be caused by: the misfit of supposed and observed physics which reduces to the inertia term in the present case, the spatial pattern of observation errors.

Through numerical tests, the most sensitive parameter of our identification algorithm (here with constant Q in space) is the lower bound of the research interval for Q (Table 3), the identification is nearly not sensitive to the first guess or the research intervals for the other parameters. The inversion of the triplet with that method is limited by the accuracy of the first guess on the low flow discharge: the error on A_0 remains low, the error on temporal discharge estimation is on the order of the error on lower discharge estimation, and the error on K greater than the error on lower discharge estimation. This first guess on discharge can be sampled randomly or given by a simple empirical formula such as the rational formula relating discharge to cumulated rainfall and drainage area (Kuichling (1889)). Alternatively, the idea of transferring discharge from gauged sites to the ungauged river section of interest can be achieved with the ratio of drainage areas as proposed by Birkinshaw et al. (2014). The sensitivity to first guess is tested in Section 5.3.

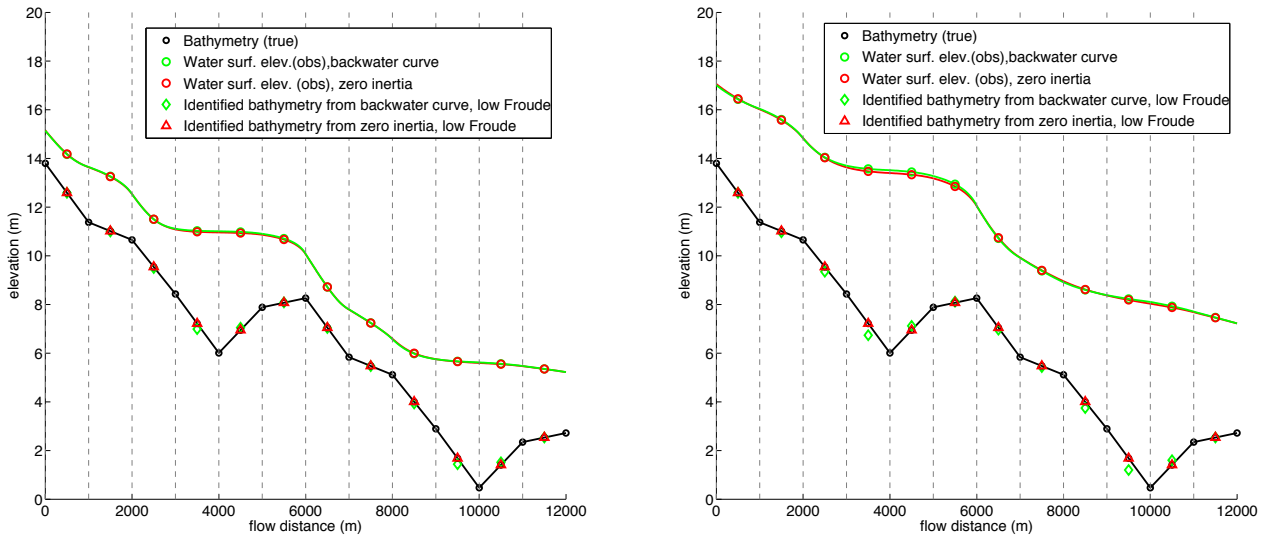

Figure 8: Bathymetry identification for the synthetic test case with low Froude model and "perfect observations", (left) $t = t_1$, (right) $t = t_3$. Continuous green and red line represent the true water surfaces calculated with the ODE solver for the backwater curve and the low Froude model. Flow features are summed up in Table 4.2 and Figure 4..

5.2 Synthetic River - bathymetry identification with method 2

The explicit model derived in Equation 3.20 is used for the inversion of bathymetry on the synthetic river test case presented in Section 4.2. First, perfect observations are used in order to test this inverse model and examine its sensitivity to the location of the depth observation that is required. After that the sensitivity of this inversion to measurement errors is investigated.

5.2.1 Inversions based on unnoised data. Analysis of the physical misfit impact

First the water depth expressed with the explicit inverse model (Equation 3.20) is solved using Method 2 exposed in Section 4.5, and with perfect observations of the river, i.e. $w_{obs} = w_{true}$, $S_{obs} = S_{true}$ and $h(x_{obs}) = h(x_{N_S})$ downstream the river reach. The identification of bathymetry is plotted for $Q_1^t = 200$ $m^3.s^{-1}$ and $Q_3^t = 700$ $m^3.s^{-1}$ (Figure 8). The red triangles represent the bathymetry identified with low Froude inverse model (Equation 3.20) from perfect observations generated with low Froude forward model (Equation 2.6). As expected since the identification is performed with the explicit inverse of the model used to generate the free surface, the identification is nearly exact and the relative error is numerical, it is on the order of 5.4×10^{-4}.

The backwater curve accounting for inertia terms (Equation 2.4) is used to generate more realistic water surface profiles. With those observations supposed perfect, the results of the low Froude inverse model are fairly good with a relative error on identified bathymetry lower than 3% (spatial average) and lower than 8% (spatial maximum) (Figure 8 and 9, green diamonds). The bathymetry error is larger where the backwater curve behaves differently than the low Froude - forward models, for example around the pools located at $x = 4000\,m$ or $x = 10000\,m$. At such locations the error on bathymetry identification is greater than the one calculated with Equation 3.22. In other words, an error on the identified bathymetry is made where inertia terms are non-negligible due to the fact that they are not accounted in the inverse model.

The influence of the location of the water depth observation $h(x_{situ})$ on the bathymetry error is tested

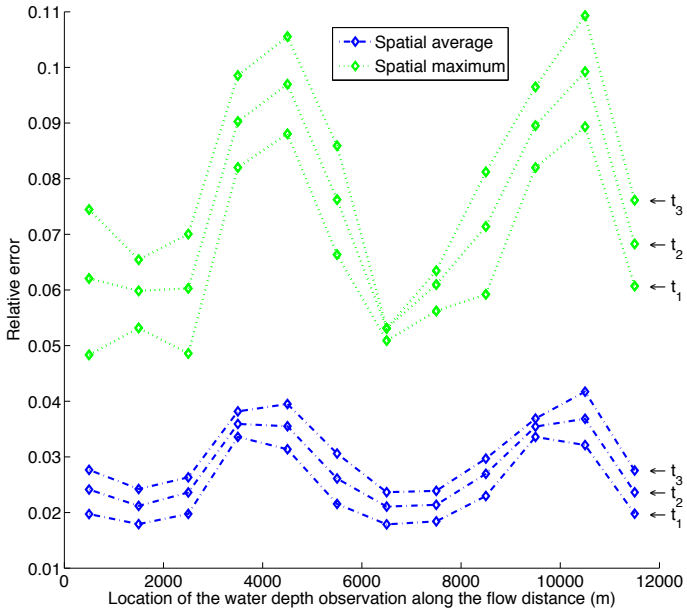

Figure 9: Mean ($\|.\|_1$) and maximum ($\|.\|_\infty$) spatial errors on bathymetry identification (low Froude inverse model, observations=backwater curve) in function of the location of the in-situ water depth measurement, "perfect observations". Flow features are summed up in Table 4.2 and Figure 4.

in Figure 9. This addresses the question of the location of the invariant $h(x_{situ})\left|w(x_{situ})S^{1/2}(x_{situ})\right|^{3/5}$which is used in the low Froude inverse model. The largest spatially averaged and maximum bathymetry errors are obtained for $t = t_3$ when the discharge is stronger. As the water depth is observed near a pool, around $x = 4000m$ or $x = 10000m$, the bathymetry errors are larger on the order of 11%. This is where the discrepancy between the low Froude approximation and the backwater curve is larger. The spatially averaged error remains lower than 4.5% for this test case which is an encouraging result. The water depth observation should be taken where the effect of inertia term is negligible at the studied scale.

5.2.2 Impact of the measurement errors on one observable

Errors on water surface width and slope measurements are simulated as exposed in Section 4.4. The low Froude inverse model (Equation 2.6) is run with those measurements; note that in-situ width and slope ($x_{situ} = x_{N_S}$) are also affected by those errors. $N_{samp} = 100$ sets of random gaussian numbers are used for each noise level, and the observations are used with the expected SWOT errors as defined in §4.4. We have: $x_{situ} = 12$ km. The impact of measurement errors on the identified bathymetry A_0 is presented in Figure 10. As expected, the amount of error due to width errors is the same for the three discharge values since the channel width is independent of time. At a width error of 15%, the error on the resulting bathymetry is 8%. At a slope error of 15% the error on bathymetry about 4%.

5.3 Synthetic Rivers - Identification of the pair (K, Q) given A_0 with method 3

From the knowledge of the low flow bathymetry, given either by the inverse model presented above or a statistical method for instance, the aim is to retrieve the two other unknowns (K, Q). The sensitivity to first

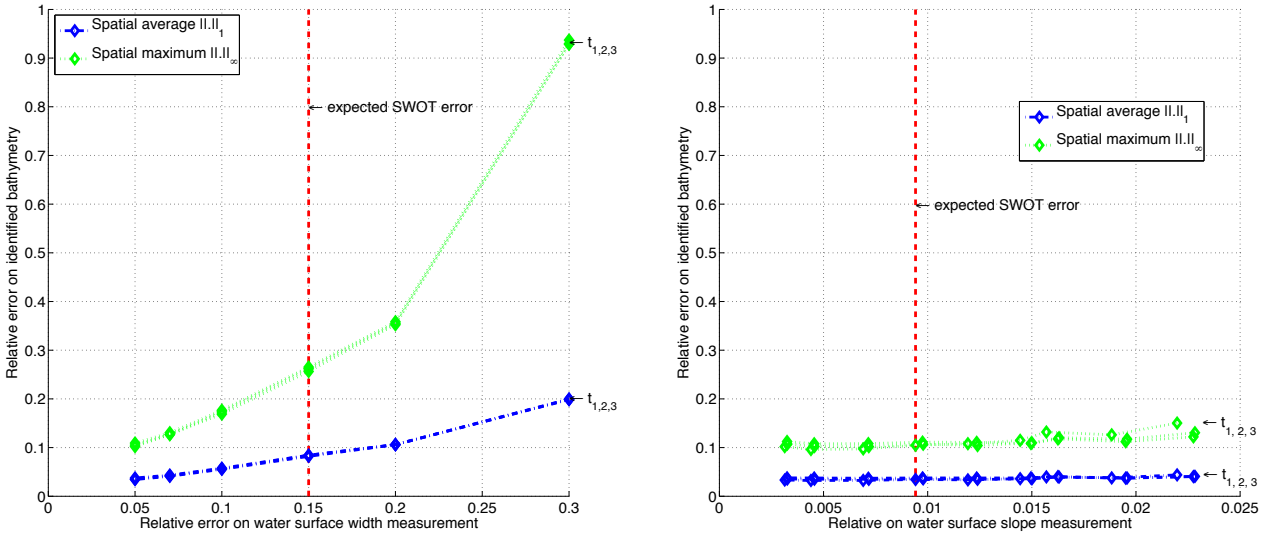

Figure 10: Sensitivity of the the identified bathymetry A_0 to measurement errors. Flow features are summed up in Table 4.2 and Figure 4.

guess on (K, Q) sought is tested on the synthetic river. Next, from a realistic first guess the identification of (K, Q) is performed on the synthetic river but also on 90 other river geometries. The sensitivity of this inversion scheme to measurement errors is investigated.

5.3.1 Sensitivity of (K, Q) identification to the first guesses

In this section, the bathymetry identified using the low Froude inverse model (Equation 3.20) is considered (and using SWOT like observations). A roughness and discharge pair (K, Q) is identified from a first guess $\left(K^b, Q^b\right)$ by solving the system (3.9) in the least square sense using Method 3, see Section 4.5. We use 3 snapshots of the synthetic river, i.e. $p = 3$, with cross-sectional water surface width constant in time. Recall that the bathymetry profile for low flow at $t = t_1$ is already identified as exposed above, and SWOT like measurements are used. The sensitivity of this algorithm to first guess is tested on a sample of 1000 random gaussian first guess such as $\left(K^{b,i} = K^t + N^i(0, 10), Q^{b,i} = Q^t + N^i(0, 250)\right)$ for $i \in [1 \dots N_{sample}]$, with true values $K^t = 20 m^{1/3}.s^{-1}$, $Q^t = (200, 400, 700)\, m^3.s^{-1}$. The results of this identifications are presented on figure 11 with the RMSE error on Q $Err_Q = {}^1/_{N_p} \left(\sum_{p=1}^{N_p} \left(Q_p - Q_p^t\right)^2\right) / \overline{Q^t} \times 100\%$, and the error on roughness $Err_K = \left(K^t - K\right) / K^t$. Two panels on the same raw can be read together since they are the projection of the same identified variable on each first guess variable. There are no obvious bias, the scatter plots are centered. Moreover the estimation of discharge is quite robust since the RMSE error rarely exceeds 50% for first guess errors up to 150% on K^b. The identification of roughness K is more sensitive to errors on first guesses Q^b and K^b.

The selection of a first guess on roughness coefficient can be done from a simple classification of rivers in function of their geomorphologic attributes (e.g. Chow (1964); Maidment (1992)). Generally river roughness lies between 10 and 40 $m^{1/3}.s^{-1}$, we use a first guess of 40 $m^{1/3}.s^{-1}$ in the following. The first guess on discharge can be given by a simple empirical formula such as the rational formula relating discharge to cumulated rainfall and drainage area (Kuichling (1889)) or other statistical methods (e.g. Birkinshaw et al. (2014)). In the following prior guessing is deliberately made with large errors, typically 100% on roughness and more than 50% on discharge.

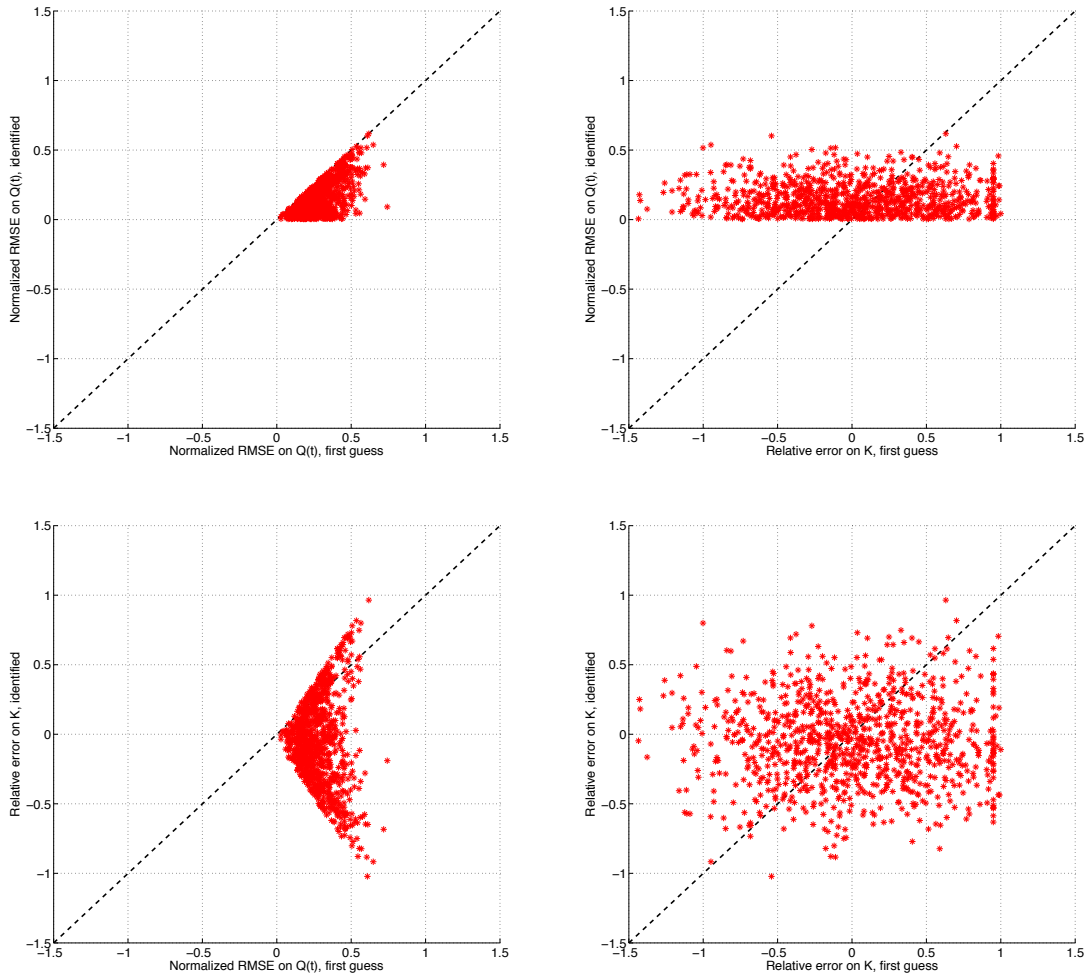

Figure 11: Sensitivity of discharge and roughness identification to first guess. Results are represented in the different planes (Err_K, Err_{K_b}), (Err_Q, Err_{Q_b}), (Err_K, Err_{Q_b}), (Err_Q, Err_{K_b}), for a sample of 1000 sets of random gaussian first guesses. Water surface observations are used with expected SWOT like errors. $x_{situ} = 12$ km. The error on K can be positive or negative. Flow features are summed up in Table 4.2 and Figure 4.

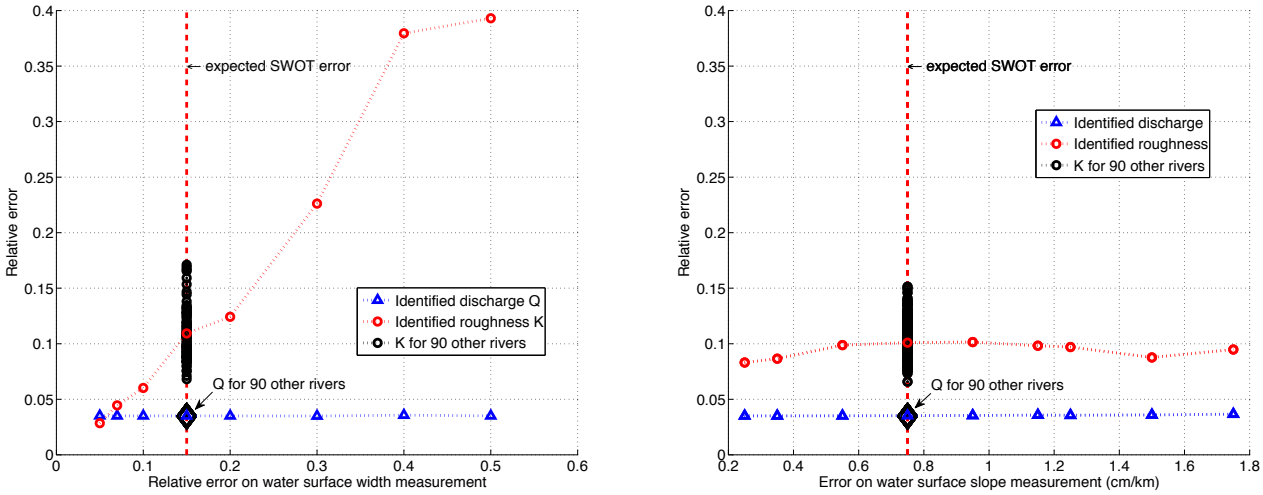

Figure 12: Sensitivity of discharge and roughness identification to measurement errors, $N_{samp} = 100$ sets of random gaussian numbers are used for each noise level. Other observations are used with expected SWOT errors as defined in Section 4.4. $x_{situ} = 12$ km. Identification are performed for 30 other channel geometries (cross sections repartitions and shapes) with the same $I_0 = 1/1000$ for discharge (black diamonds) and roughness (black circles), 60 other geometries with $I_0 = 0.5/1000$ and $I_0 = 0.1/1000$.

5.3.2 Sensitivity of (K, Q) identification to the measurement errors

For the synthetic test cases, first guesses on discharge and roughness are $(K_b, Q_b^1, Q_b^2, Q_b^3) = (40, 500, 500, 500)$, while the true values are $(K_t, Q_t^1, Q_t^2, Q_t^3) = (20, 200, 400, 700)$; hence first guess RMSE on discharge time series is 50% and 100% on roughness. As shown on Figure 12 the identification of discharge (constant in space) is quite robust with a RMSE of 3.5% and rather insensitive to measurement errors. This is also true for 90 other river geometries, with mean slopes ranging from 10^{-4} m/m to 10^{-3} m/m and contrasted bottom and cross sectional geometries, producing various flow configurations. The identification of roughness is more sensitive to measurement errors with a relative error on roughness about 10% and $\pm 5\%$ spreading depending on the river geometry. Different first guesses on roughness K from 10 to 40 $m^{1/3}.s^{-1}$ were also tested and the discharge identification remains insensitive, the relative error on roughness is approximately the same than before.
The robustness of discharge estimation may stem from three reasons:

- The observation grid, here at $1km$, imposes a representation of the flow and consequently of the Froude number which is a local quantity. In this Froude range (cf. Table 4.2), the low Froude model reveals to be sufficient to obtain an accurate estimation of discharge with a 3.5% RMSE.
- The amount of information brought by temporal revisits and which reveals to be a good constraint to solve the pair (K, Q).
- The fact that the cross section is rectangular both for forward and inverse models; the error on wetted cross sectional area only comes from measurement errors and from the misfit between supposed and observed physical complexity. This will be investigated after.

5.4 Garonne river test case

The accuracy of the approach is validated on a SWOT scenario for the Garonne River downstream of Toulouse. A bathymetry identification is performed with the explicit inverse model (equation 3.20) solved using Method 2 exposed in Section 4.5, an observation point is taken downstream of the river section at $x = 75.7$ km. First, based on the identified bathymetry, the pair (K, Q) is identified by solving the system (3.9) using Method 3 presented in Section 4.5. Next, an identification of the triplet (A_0, K, Q) is also performed from SWOT like measurements only, the system (3.9) is solved using Method 1b presented in Section 4.5. SWOT like measurements are obtained by adding noise to variables simulated with a backwater curve equation for each reach as explained in Section 4.4. The identifications are first performed for 3 SWOT-like observations to be able to compare the results with those from the previous sections; but also for a 10 days hydrograph to study a larger range of hydraulic regimes and river behaviors.

5.4.1 Effective bathymetry identification with method 2)

Figure 13 shows the low flow line simulated with forward backwater curve and a rectangular cross section on each reach, i.e. a succession of permanent states used as SWOT like observations. It is in fairly good agreement with the reference flow line from 1D shallow water (unsteady) model running on real cross sections. Figure 13 shows the identification of bathymetry using Equation (3.20) for 80 km of the Garonne River from SWOT like observations and one observation point. The comparison between identified and true bathymetry is fairly good for the whole river domain. The relative error of identification on effective bathymetry is 1% on average in space with a maximum error of 3% and is due to: a) the measurement errors (SWOT like errors added to backwater curve for each reach); b) the misfit between observed and supposed physics (inertial terms, unsteady flow). The results of bathymetry identification with low Froude inverse model are fairly good for low flows such as the one considered here on the Garonne River around $160m^3.s^{-1}$ with $\partial_x Q$ close to 0. If the spatial variation of discharge $\partial_x Q$ is significant along the studied domain (it is not the hypothesis of the inverse model), a bias on bathymetry identification appears and increases for river sections far from the observation point.

5.4.2 Inversion of the pair (K, Q) given $A_0$with method 3)

From the bathymetry identified above and water surface width measurements, A_0 can be calculated and is plotted along the flow distance in Figure 14 (right). Recall that the roughness and discharge (K, Q) are identified from a first guess (K_b, Q_b) by solving the system (3.9) in the least square sense using Method 3, see Section 4.5. The RMSE on first guess for discharge Q is 65% while the final RMSE on discharge is 5%. The relative error on roughness K is +100% overestimation for the first guess and falls to +50% after identification. Figure 14 (right) shows the estimation error on A_0, the relative error being 1% on average in space with a maximum error of 3%. The relative error on wetted surface A for the third observation time is 1% on average in space with a maximum error of 5%.

From the spatial error on discharge and the pattern of estimated cross sectional areas at the third observation time t_3, the larger errors on discharge are for reaches around 35 km for which the cross section variation between low flow and high flow is the largest, about a factor 3. The observation errors on w, S, Z are also involved. But as stated before, a large part of overestimation of the roughness K might be apportioned to the misfit between the observed physics and the simplified hypothesis of the inverse model.

Figure 15 shows the discharge identified within the pair (K, Q) for 11 days on the Garonne River. The average RMSE is 53% for the first guess on discharge and +100% overestimation for the first guess on roughness. The identification is fairly efficient and the errors falls at 14.3% mean RMSE on discharge and +36% on the roughness K. This identification is performed for SWOT like observations for $1km$ reaches and for $5km$ reaches, hence 5 observations are averaged for each reach. In both cases the lower discharges tend to be underestimated compared to a more accurate peak flow estimation. As shown on Figure 15, the spreading

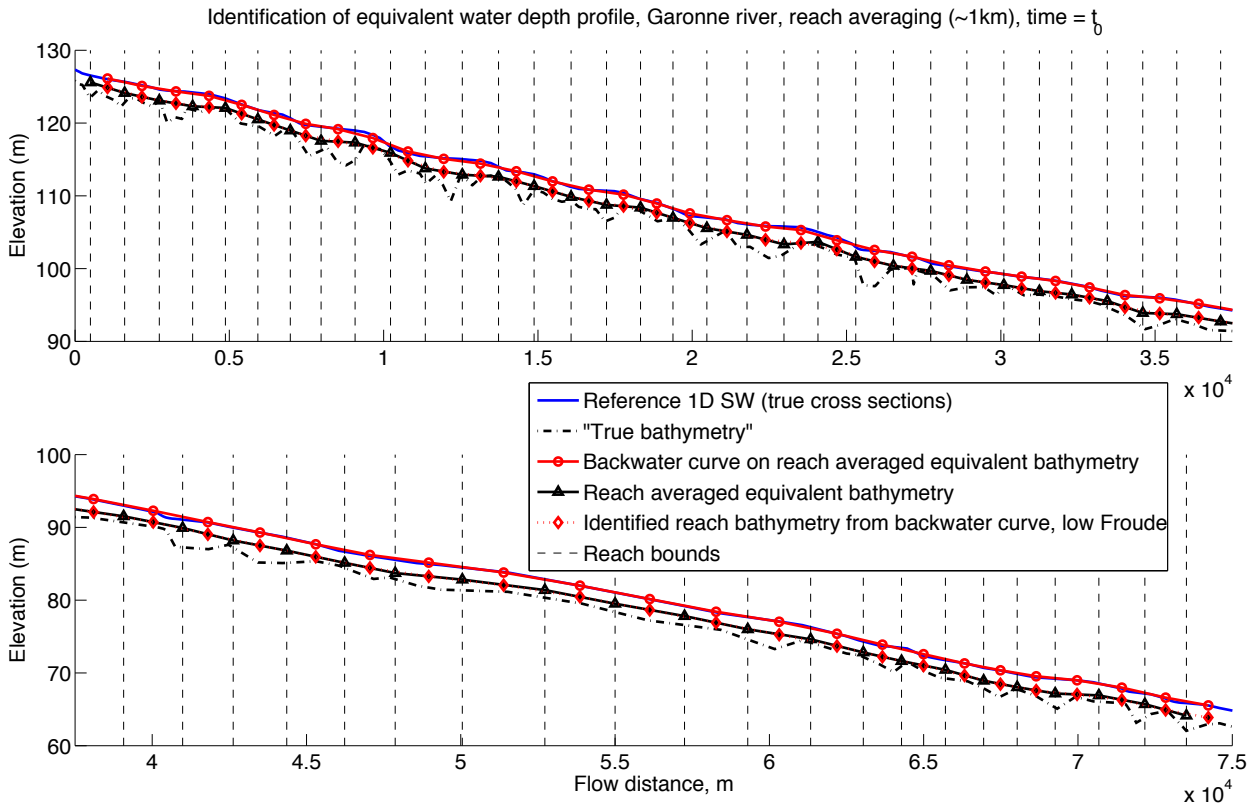

Figure 13: effective bathymetry identification for low flow on the Garonne River downstream of Toulouse on the 09/01/2004. The mean absolute error is 1% and the spatial maximum is 3%.

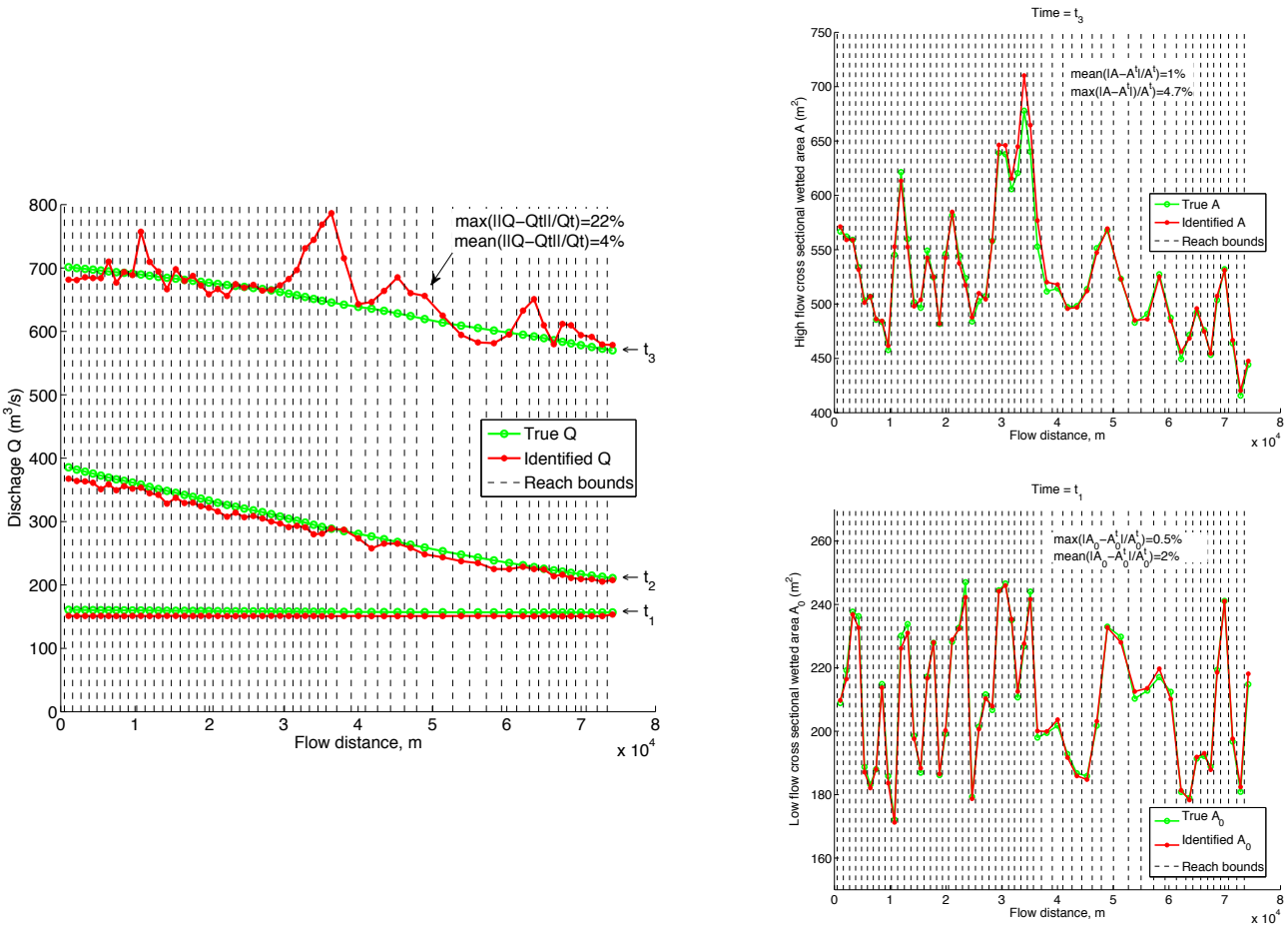

Figure 14: Identification of (K, Q) given A_0 for the 9^{th} to the 11^{th} of January 2004: (Left) Identified discharge along the flow distance for the Garonne River downstream of Toulouse ; first guess is $(K_b, Q_b^1, Q_b^2, Q_b^3) = (40, 500, 500, 500)$ with SWOT like observations, $RMSE = 3\%$. The uniform roughness identified is $K = 29.9$, true uniform roughness being $K_t = 20$. (Right, top) Low flow rectangular cross sectional area A_0 with bathymetry identification from low Froude model and SWOT like observations, (right, bottom) cross sectional area estimated at $t = t_1$ from A_0 and SWOT like measurements.

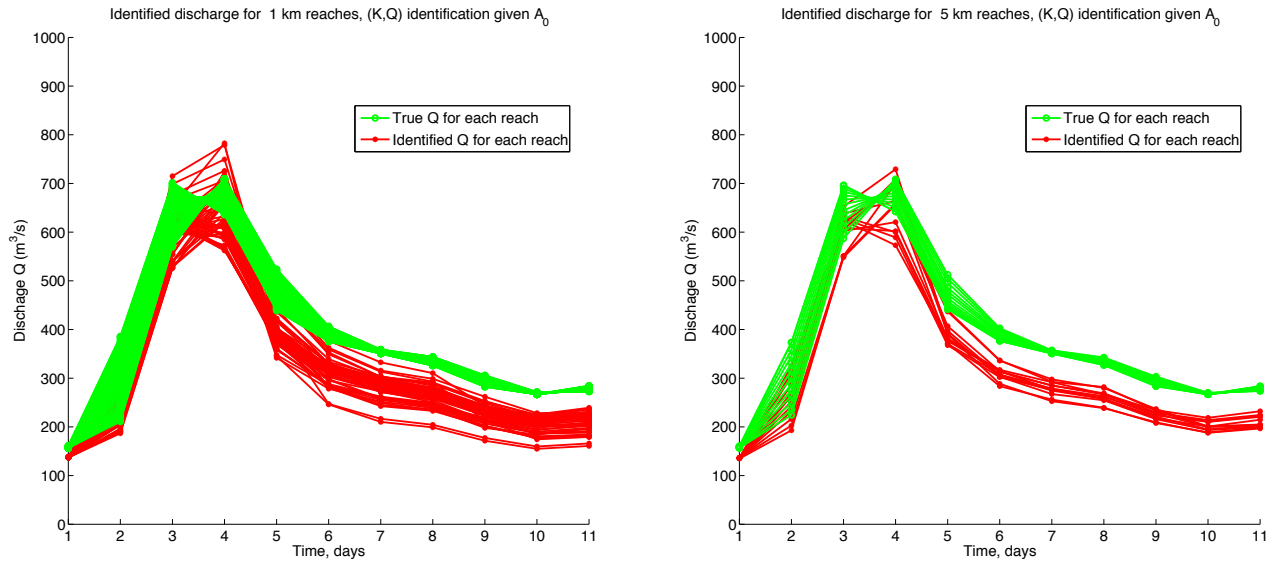

Figure 15: Identification of (K, Q) given A_0 for the 9^{th} to the 20^{th} of January 2004 for each reach: identified discharge along the flow distance for the Garonne River; first guess is $(K_b, Q_b^1, Q_b^2, Q_b^3) = (40, 400, 400, 400)$ with SWOT like observations, (left) for $1km$ reaches and (right) for $5km$ reaches (hence 5 observation values are averaged for each reach). In both cases spatially averaged $RMSE = 14.3\%$ on discharge and the relative error on the roughness K is $+36\%$. Each set of curve represents the spreading of reach behaviors along the flow distance.

of identified discharges is smaller for longer reaches. One reason might be the hydraulic behavior of reaches, and so their unicity, which tend to be smoothed for increasing averaging distances.

5.4.3 Inversion of the triplet (A_0, K, Q) with method 1b)

From SWOT like observations only, the triplet formed by low flow bathymetry, roughness and discharge (K, Q, A_0) is identified from a first guess $\left(A_0^b, K^b, Q^b\right)$ by solving the system (3.9) in the least square sense using Method 1b, Section 4.5. Figure 16 shows the discharge identified within the triplet for 11 days on the Garonne River. The average RMSE is 53% for the first guess on discharge, $+100\%$ overestimation for the first guess on roughness and -20% underestimation for A_0. The identification of discharge is fairly good with an error of 14.1% RMSE. However the identification of the other flow parameters is less efficient with an underestimation of -43% for the roughness K and a $+65\%$ underestimation for A_0. Interestingly, the underestimation of K is somehow compensated by an overestimation of A_0 or conversely. In other words, it corresponds to different effective roughness/geometry pairs also called effective roughness/geometries. Indeed, if re-computing the discharge from the identified K and A_0 (like it has been done in § 5.1.2), the RMSE averaged in space remains nearly the same about 14%.

6 Conclusion

The important question of unobservable river flow parameters and their identifiability have been addressed given SWOT like data - spatially and temporally distributed measurements of river surface elevation, width and slope. The inference of low flow bathymetry, roughness and discharge (A_0, K, Q) have been investigated through the analysis of inverse models of decreasing complexity. All the inverse models elaborated and

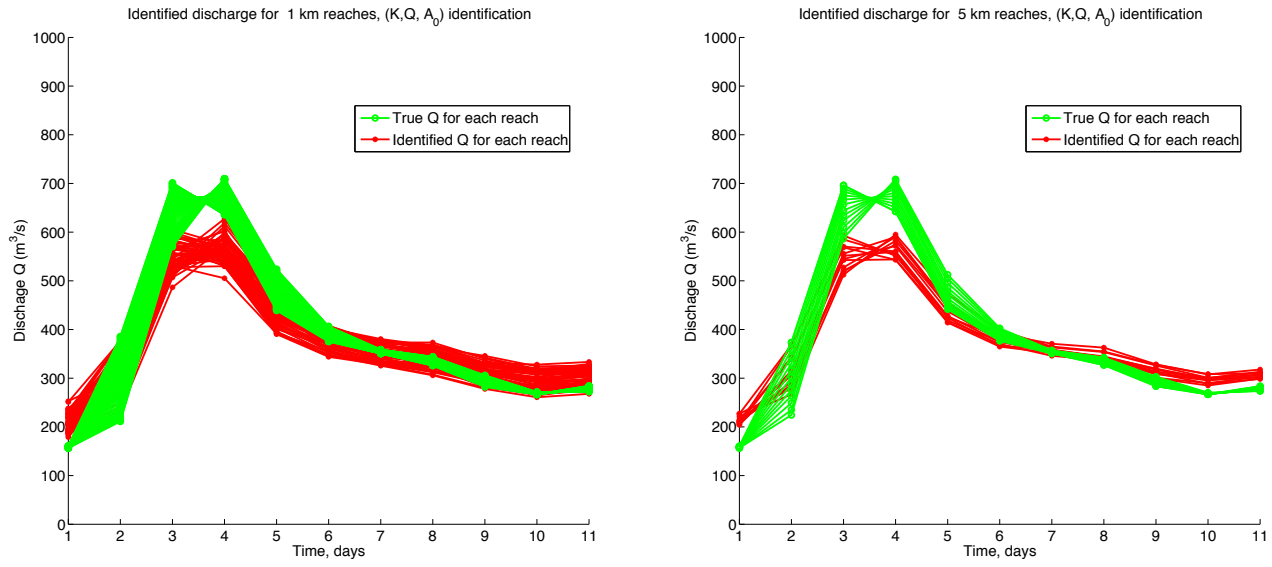

Figure 16: Identification of (A_0, K, Q) given for the 9^{th} to the 20^{th} of January 2004 for each reach: identified discharge along the flow distance for the Garonne River downstream Toulouse ; $(A_{0b}, K_b, Q_b^1, Q_b^2, Q_b^3) = (250, 40, 400, 400, 400)$ with SWOT like observations, (left) for $1km$ reaches and (right) for $5km$ reaches (hence 5 observation values are averaged for each reach). In both cases spatially averaged $RMSE = 14.1\%$ on discharge and the relative error on the roughness K is -43% and the error on A_0 is $+65\%$ Each set of curve represents the spreading of reach behaviors along the flow distance.

performed are deterministic and solved using simple, hence well controlled, numerical algorithms. The concept of an effective cross sectional bathymetry and roughness has been proposed to represent the unobservable part of a river reah - below the lowest flow observed. Next an effective topography-friction pair modeling accurately the river flow can be infered in the range of the observed flow variability. Moreover it has been shown that inversion models including the inertia terms require an unrealistic data resolution, while the most complete physical model allowing to separate the roughness coefficient from the bathymetry is the low Froude model**.** Two approaches are proposed for infering the river properties (A_0, K, Q) depending on the observations available: Case 1) remotely sensed observations of river surface only are available; 2) the same remotely sensed observations are available plus one (1) in-situ depth measurement. The different inverse models elaborated have been assessed precisely on 91 synthetic test cases sampling a wide range of river configurations but also on the Garonne River (France) characterized by large spatio-temporal variabilities.

In Case 1), the identification of the triplet (A_0, K, Q) from a first guess in the least square sense for three and eleven river snapshots in time gave fairly good discharges estimations with RMSE around 15% both on the Garonne River and on a large set of synthetic rivers. Interestingly, compensations between the identified values of K and A_0 are obtained, and the existence of effective roughness - geometry pairs for a given discharge hydrograph is highlighted.

The fundamental issue of identifying the river bathymetry, in fact a rectangular one with the same wetted surface, has been addressed. In Case 2), given an extra in-situ water depth measurement, a method for identifying a bathymetry profile based on effective rectangular sections, is proposed. In the case of the Garonne River, the error on the identification of effective river depth profile is 1% on average in space with a maximum error of 3%. Next, given these effective low flow cross sectional areas along the flow distance, an identification of the pair (K, Q), instead of the triplet as in Case 1), can be addressed. Based on the inverse models elaborated, the following inversion accuracy are obtained on the Garonne River: a RMSE of 5% for a 3 days rising hydrograph and a 14.3% RMSE for a 11 days flood with its recession. In this case, the effective low flow area A_0 is accurate, but it is the identified roughness coefficient K with a relative error of 50%

which contains the misfit between the observed reality and the inverse model assumptions.

An important feature of the present inverse methods is the fairly good accuracy of the discharge Q obtained, while the identified roughness coefficient K includes: the measurement errors and the misfit of physics between the real flow dynamics and the inverse model hypothesis, which mainly comes from the unsteadiness of the observed flow and inertia effects. In other respect, defining river reaches from a SWOT-like observation grid averages the river properties in each reach, hence tends to smooth the hydraulic variability. In particular, the representation of the flow control sections, including those responsible for local hydraulic singularities, depends on the resolution of the observation grid. Finally, the present study suggests forthcoming work aiming at estimating the discharge for a large range of hydrosystems, in order to investigate effective topography-friction pairs, especially for more complex flows such as braided rivers for example.

7 Acknowledgments

The authors gratefully acknowledge Hélène Roux from Institut de Mécanique des Fluides de Toulouse (IMFT), Denis Dartus, Kevin Larnier and Jacques Chorda, IMFT, for the numerous fruitful discussions and the Garonne data support; also, Sylvain Biancamaria from Laboratoire d'Etudes en Géophysique et Océanographie Spatiale (LEGOS) for fruitful discussions related to SWOT type data features.The first author has been funded by CNES (Centre National d'études Spatiales), postdoctoral and TOSCA grant.

8 References

References

Aronica, G., Hankin, B., Beven, K., 1998. Uncertainty and equifinality in calibrating distributed roughness coefficients in a flood propagation model with limited data. Advances in Water Resources 22, 349–365, 4.

Biancamaria, S., Andreadis, K. M., Durand, M., Clark, E. A., Rodriguez, E., Mognard, N. M., Alsdorf, D. E., Lettenmaier, D. P., Oudin, Y., 2010. Preliminary characterization of SWOT hydrology error budget and global capabilities. Selected Topics in Applied Earth Observations and Remote Sensing, IEEE Journal of 3, 6–19, 1.

Biancamaria, S., Durand, M., Andreadis, K. M., Bates, P. D., Boone, A., Mognard, N. M., Rodriguez, E., Alsdorf, D. E., Lettenmaier, D. P., Clark, E. A., 2011. Assimilation of virtual wide swath altimetry to improve arctic river modeling. Remote Sensing of Environment 115, 373–381, 2.
URL http://www.sciencedirect.com/science/article/pii/S0034425710002816

Birkinshaw, S. J., Moore, P., Kilsby, C., O'Donnell, G. M., Hardy, A., Berry, P. A. M., 2014. Daily discharge estimation at ungauged river sites using remote sensing. Hydrological Processes 28 (3), 1043–1054.
URL http://dx.doi.org/10.1002/hyp.9647

Bjerklie, D. M., Dingman, S. L., Vorosmarty, C. J., Bolster, C. H., Congalton, R. G., 2003. Evaluating the potential for measuring river discharge from space. J. of Hydrology 278, 17–38.

Bjerklie, D. M., Moller, D., Smith, L. C., Dingman, S. L., 2005. Estimating discharge in rivers using remotely sensed hydraulic information. Journal of Hydrology 309, 191–209, 1-4.
URL http://www.sciencedirect.com/science/article/pii/S0022169404005724

Bélanger, E., Vincent, A., 2005. Data assimilation (4d-var) to forecast flood in shallow-waters with sediment erosion. Journal of Hydrology 300 (1?4), 114 – 125.
URL http://www.sciencedirect.com/science/article/pii/S0022169404002914

Carlier, M., 1982. Hydraulique générale et appliquée. Eyrolles, Paris, France.

Chow, V., 1959. Open-channel Hydraulics. Mc Graw-Hill, New-York, USA.

Chow, V., 1964. Handbook of applied hydrology. McGraw-Hill Book Co., New-York, 1467 pages.

Durand, M., Neal, J., Rodriguez, E., Andreadis, K. M., Smith, L. C., Yoon, Y., 2014. Estimating reach-averaged discharge for the river severn from measurements of river water surface elevation and slope. Journal of Hydrology - (0), –.
URL http://www.sciencedirect.com/science/article/pii/S002216941400002X

Durand, M., Rodriguez, E., Alsdorf, D. E., Trigg, M., 2010. Estimating river depth from remote sensing swath interferometry measurements of river height, slope, and width. Selected Topics in Applied Earth Observations and Remote Sensing, IEEE Journal of 3, 20–31, 1.

Frappart, F., Calmant, S., Cauhopé, M., Seyler, F., Cazenave, A., 2006. Preliminary results of {ENVISAT} ra-2-derived water levels validation over the amazon basin. Remote Sensing of Environment 100 (2), 252 – 264.
URL http://www.sciencedirect.com/science/article/pii/S0034425705003585

Gessese, A., 2013. Algorithms for bed topography reconstruction in geophysical flows. Ph.D. thesis, University of Canterbury. Mechanical Engineering.
URL http://ir.canterbury.ac.nz/handle/10092/8673

Gessese, A., Wa, K., Sellier, M., 2013. Bathymetry reconstruction based on the zero-inertia shallow water approximation. Theoretical and Computational Fluid Dynamics 27 (5), 721–732.
URL http://dx.doi.org/10.1007/s00162-012-0287-5

Gessese, A. F., Sellier, M., Houten, E. V., Smart, G., 2011. Reconstruction of river bed topography from free surface data using a direct numerical approach in one-dimensional shallow water flow. Inverse Problems 27 (2), 025001.
URL http://stacks.iop.org/0266-5611/27/i=2/a=025001

Han, S.-C., Shum, C., Braun, A., 2005. High-resolution continental water storage recovery from low-low satellite-to-satellite tracking. Journal of Geodynamics 39 (1), 11 – 28.
URL http://www.sciencedirect.com/science/article/pii/S026437070400095X

Honnorat, M., 2007. Assimilation de données lagrangiennes pour la simulation numérique en hydraulique fluviale. phd thesis, INPG, Grenoble, France.
URL http://www-ljk.imag.fr/membres/Marc.Honnorat/these/index.html

Honnorat, M., Lai, X., le Dimet, F.-X., Monnier, J., 2006. Variational data assimilation for 2D fluvial hydraulics simulation. CMWR XVI-Computational Methods for Water Ressources. Copenhagen, june 2006. Pearl river test case.

Honnorat, M., Monnier, J., Dimet, F.-X., 2009. Lagrangian data assimilation for river hydraulics simulations. Computing and Visualization in Science 12 (5), 235–246.
URL http://dx.doi.org/10.1007/s00791-008-0089-x

Honnorat, M., Monnier, J., Rivière, N., Huot, t., Le Dimet, F.-X., 2010. Identification of equivalent topography in an open channel flow using lagrangian data assimilation. Computing and Visualization in Science 13 (3), 111–119.
URL http://dx.doi.org/10.1007/s00791-009-0130-8

Hostache, R., Lai, X., Monnier, J., Puech, C., 2010. Assimilation of spatially distributed water levels into a shallow-water flood model. part II: use of a remote sensing image of mosel river. Journal of Hydrology 390, 257–268, 3-4.
URL http://www.sciencedirect.com/science/article/pii/S0022169410004166

Jowett, I. G., 1993. A method for objectively identifying pool, run, and riffle habitats from physical measurements. New Zealand Journal of Marine and Freshwater Research 27 (2), 241–248.
URL http://dx.doi.org/10.1080/00288330.1993.9516563

Jung, H. C., Hamski, J., Durand, M., Alsdorf, D., Hossain, F., Lee, H., Hossain, A. K. M. A., Hasan, K., Khan, A. S., Hoque, A. Z., 2010. Characterization of complex fluvial systems using remote sensing of spatial and temporal water level variations in the amazon, congo, and brahmaputra rivers. Earth Surface Processes and Landforms 35 (3), 294–304.
URL http://dx.doi.org/10.1002/esp.1914

Kuichling, E., 1889. The relation between the rainfall and the discharge of sewers in populous districs. ASCE.

Lai, X., Monnier, J., 2009. Assimilation of spatially distributed water levels into a shallow-water flood model. part i: Mathematical method and test case. Journal of Hydrology 377, 1–11, 1-2.
URL http://www.sciencedirect.com/science/article/pii/S0022169409004508

Larnier, K., 2010. Modélisation thermohydraulique d'un tronçon de garonne en lien avec l'habitat piscicole : approches statistique et déterministe. Ph.D. thesis, Toulouse.

Maidment, D. R., 1992. Handbook of hydrology.

Moré, J., 1977. The Levenberg-Marquardt Algorithm: Implementation and Theory. Springer.

Moré, J., Sorensen, D., 1983. Computing a trust region step. SIAM Journal on Scientific and Statistical Computing 4 (3), 553–572.
URL http://epubs.siam.org/doi/abs/10.1137/0904038

Munier, S., Palanisamy, H., Maisongrande, P., Cazenave, A., Wood, E. F., 2012. Global runoff anomalies over 1993?2009 estimated from coupled land?ocean?atmosphere water budgets and its relation with climate variability. Hydrology and Earth System Sciences 16 (10), 3647–3658.
URL http://www.hydrol-earth-syst-sci.net/16/3647/2012/

Negrel, J., Kosuth, P., Bercher, N., 2011. Estimating river discharge from earth observation measurements of river surface hydraulic variables. Hydrology and Earth System Sciences 15 (6), 2049–2058.
URL http://www.hydrol-earth-syst-sci.net/15/2049/2011/

Rodriguez, E., 2012. SWOT science requirements document. JPL document, JPL.

Romeiser, R., Runge, H., Suchandt, S., Sprenger, J., Weilbeer, H., Sohrmann, A., Stammer, D., Dec 2007. Current measurements in rivers by spaceborne along-track insar. Geoscience and Remote Sensing, IEEE Transactions on 45 (12), 4019–4031.

Roux, H., 2004. Estimation de paramètres en hydraulique fluviale, à partir de données caractéristiques de l'imagerie aérienne. Thèse de doctorat, Institut National Polytechnique de Toulouse, Toulouse, France.

Roux, H., Dartus, D., 2005. Parameter identification using optimization techniques in open-channel inverse problems. J. of Hyd. Res. 43, 311–320, 3.

Roux, H., Dartus, D., 2006. Use of parameter optimization to estimate a flood wave: Potential applications to remote sensing of rivers. J. of Hydrology 328, 258–266.

Roux, H., Dartus, D., Jul. 2008. Sensitivity analysis and predictive uncertainty using inundation observations for parameter estimation in open-channel inverse problem. J. Hydr. Eng. ASCE 134, 541–549, 5.

Simeoni-Sauvage, S., 1999. Modélisation hydrobiogéochimique de la garonne à l'étiage estival : cas de l'azote entre toulouse et agen (120 kilomètres). Ph.D. thesis, Toulouse, INPT.

Strelkoff, T., Clemmens, A., 2000. Approximating wetted perimeter in power-law cross section. Journal of Irrigation and Drainage Engineering 126 (2), 98–109.

Tarpanelli, A., Brocca, L., Melone, F., Moramarco, T., 2013. Hydraulic modelling calibration in small rivers by using coarse resolution synthetic aperture radar imagery. Hydrological Processes 27 (9), 1321–1330.
URL http://dx.doi.org/10.1002/hyp.9550

Yoon, Y., Durand, M., Merry, C. J., Clark, E. A., Andreadis, K. M., Alsdorf, D. E., 2012. Estimating river bathymetry from data assimilation of synthetic {SWOT} measurements. Journal of Hydrology 464 - 465 (0), 363 – 375.
URL http://www.sciencedirect.com/science/article/pii/S0022169412006294

9 Annex

The Annex contains few enriched inverse models or instructive expressions investigated:

- explicit roughness coefficient expression with the inertia term,
- complete one-equation model for permanent flows re-written in view of bathymetry-friction inversion,
- the low Froude model in view of explicit bathymetry identification but with general hydraulic radius.

9.1 Explicit roughness coefficient expression with the inertia term

The goal in this section is to derive the explicit expression of the roughness coefficient K resulting from Equation (2.4) and in function of the SWOT like observables. From recasting Equation (2.4), it writes:

$$\left\{ \begin{array}{l} Q_{1,p} = ... = Q_{N_R,p} \\ Q_{r,p}^2 = \dfrac{gK^2 A_{r,p}^3 \left. R_h^{4/3}\right|_{r,p} S_{r,p}}{K^2 w_{r,p} \left. R_h^{4/3}\right|_{r,p} \left.\partial_x h\right|_{r,p} - gA_{r,p}} \end{array} \right. \quad \forall r \in [1..N_r], \forall p \in [1..N_p] \tag{9.1}$$

From this system, the following equality for two river reaches holds:

$$\frac{gK^2 A_{r,p}^3 \left. R_h^{4/3}\right|_{r,p} S_{r,p}}{K^2 w_{r,p} \left. R_h^{4/3}\right|_{r,p} \left.\partial_x h\right|_{r,p} - gA_{r,p}} = \frac{gK^2 A_{r+1,p}^3 \left. R_h^{4/3}\right|_{r+1,p} S_{r+1,p}}{K^2 w_{r+1,p} \left. R_h^{4/3}\right|_{r+1,p} \left.\partial_x h\right|_{r+1,p} - gA_{r+1,p}} \text{ for } r \in [1 \cdots N_r - 1].$$

Then, the explicit expression of the roughness coefficient, given by two observed reaches, writes:

$$K_{r,r+1}^2 = g \frac{\chi_r - \chi_{r+1}}{\chi_r \psi_{r+1} - \chi_{r+1} \psi_r} \tag{9.2}$$

with $\chi_r = A_{r,p}^3 \left. R_h^{4/3}\right|_{r,p} S_{r,p}$, $\psi_r = w_{r,p} \left. R_h^{4/3}\right|_{r,p} \left.\partial_x h\right|_{r,p}$ and $(w_{r,p}, S_{r,p})$ observed quantities.

Given $A_{0,r}$, consequently$A_{r,p}$ and the hydraulic radius R_h, the numerical tests we performed revealed that this explicit expression of K is very sensitive to measurement errors. Furthermore, since the estimation of $\left.\partial_x h\right|_r$ for each reach is required, this expression is unfortunatly useless in the present observation accuracy context.

9.2 Complete one-equation model for bathymetry-friction inversion

In this section, the complete one-equation model in depth h variable for permanent flows is recalled. In the present inversion context, it demonstrates that the most complete physical model allowing to separate the bathymetry inversion from the friction coefficient one, is the low Froude model, i.e. if the Froude number small enough (typically $Fr < 0.3$ implies $(1-Fr^2)^{-1} \approx 1$ at 10%). The steady-state 1D Saint-Venant equations with no lateral inflow and with α/K^2 as the weight coefficient for inertia term, writes:

$$\partial_x Q = 0 \tag{9.3}$$

$$\frac{\alpha}{K^2} \partial_x \left(\frac{Q^2}{A} \right) + gA \left(\partial_x Z + \frac{Q\,|Q|}{K^2 A^2 R_h^{4/3}} \right) = 0 \tag{9.4}$$

The Saint-Venant equation are retrieved by setting: $\alpha = K^2$. The coefficient α is introduced for a sake of clarity in view to distinguish the inertia terms from others. This equations system is re-written in the one equation model form such as lubrication-like models. The following assumptions are made:

- the river/channel is wide enough to consider: $R_h \approx h$
- cross sections are rectangular: $A = wh$
- The Strickler roughness coefficient K is supposed constant in space
- The sign of Q is known, and supposed positive for the sake of simplicity. In other words the channel flows with increasing distance.
- The free surface slope is monotonous and non-flat: $\partial_x Z > 0$

Then, Q^2 can be written:

$$Q^2 = K^2 \frac{g w(x)^3 h(x)^{10/3} \partial_x Z(x)}{\alpha h(x)^{4/3} \partial_x w(x) + \alpha h(x)^{1/3} w(x) \partial_x h(x) - g w(x)} \tag{9.5}$$

if $h(x)\partial_x w(x) + w(x)\partial_x h(x) - g w(x) \neq 0$.

Mass conservation equation gives: $\partial_x Q^2 = 0$. By denoting: $Q^2 = {}^{Num}/_{Den}$, the last equation writes: $Den \times \partial_x Num - Num \times \partial_x Den = 0$.

After simplifications, the one-equation model in h (lubrication type) writes:

$$\alpha h'' - 3\alpha \frac{(h')^2}{h} + \left[-\alpha \left(4\frac{w'}{w} + \frac{Z''}{Z'} \right) + \frac{10}{3} \frac{g}{h^{4/3}} \right] h' + \alpha \left[-3 \left(\frac{w'}{w} \right)^2 - \frac{w'}{w}\frac{Z''}{Z'} + \frac{w''}{w} \right] h + \frac{2g}{h^{1/3}} \frac{w'}{w} + \frac{g}{h^{1/3}} \frac{Z''}{Z'} = 0 \tag{9.6}$$

Recall that the quantities Z, w and $\partial_x Z$ are given data.

The one-equation model is a second order non-linear differential equation which can be written as:

$$h'' = \left(3\frac{h'}{h} + 4\frac{w'}{w} + \frac{Z''}{Z'} \right) h' + \left(3 \left(\frac{w'}{w} \right)^2 + \frac{w'}{w}\frac{Z''}{Z'} - \frac{w''}{w} \right) h - \frac{g}{\alpha} \left(\frac{10}{3}\frac{h'}{h} + 2\frac{w'}{w} + \frac{Z''}{Z'} \right) h^{-1/3} \tag{9.7}$$

Few remarks can be made.

Given the true value of $\alpha = K^2$, given very dense and accurate observations of water surface width w, elevation Z, and river depth profile (h, h') at one location point, an accurate numerical scheme (ie Runge-Kutta high-order method) provides the river depth profile. But since, first order derivatives w', Z' and h' are needed, also second order derivatives w'', Z'' in the whole domain, it is absolutly unrealistic in the present geophysical context to solve this second order differential equation.

In other respects, Equation (**3.20**) shows that the low Froude model without inertia terms (i.e. the case $\alpha = 0$) is the most complete physical model which allows to separate the bathymetry terms from the friction ones. Based on this remark, given the low Froude model, it is possible to infer the bathymetry independently of the friction coefficient K; furthermore, it is possible to derive an explicit expression of the river depth profile h. The later derivation is done in Section 3.5.

9.3 Low Froude case and bathymetry identification with general hydraulic radius

The aim of this section is to demonstrate that an a-priori hypothesis on the low flow cross sectional shape is required in order to find an explicit expression of the river depth profile, see Section **3.5.** To our best knwowledge, the explicit expression of the bathymetry independent of the roughness coefficient has been presented first in Gessese et al. (2013). In the later the expression is derived in the 2D stationnary case with

no advection term (zero-inertia) both for the forward and inverse models. The original study led in Gessese et al. (2013) was limited to test cases with very simple and smooth geometries and fine grid resolutions. In other respect, it has been demonstrated in the previous section that the zero-inertia model (called Gessese et al. (2013)) is the most complete physical model which allows to separate the bathymetry terms from the friction ones. Below, the explicit expression of h is derived in a real-like geometries context.

Low Froude indicates the assumption $Fr^2 \ll 1$, hence $(1 - Fr^2) \approx 1$. The 1D steady-state Saint-Venant model writes:

$$\partial_x Q = 0 \tag{9.8}$$

$$\partial_x h + \partial_x b + \frac{Q\,|Q|}{K^2 A^2 R_h^{4/3}} = 0 \tag{9.9}$$

With $h(x)$ the water depth and $b(x)$ the river bed elevation, x being the spatial coordinate. Recall that the quantities Z, w and $\partial_x Z$ are given data. The roughness coefficient K is assumed to be constant in space. The free surface is assumed monotonous and non-flat free surface slope, flow from left to right, i.e. $\partial_x Z < 0$. Then, it can be deduced that :

$$Q = -\frac{\partial_x Z}{\sqrt{|\partial_x Z|}} K A R_h^{2/3} \tag{9.10}$$

Substituting equation (9.10) into equation (9.8) gives:

$$\partial_x \left(-\frac{\partial_x Z}{\sqrt{|\partial_x Z|}} K A R_h^{2/3} \right) = 0 \tag{9.11}$$

Hence:

$$\frac{2}{3} \frac{\partial_x Z}{\sqrt{|\partial_x Z|}} A R_h^{-1/3} \partial_x \left(R_h\right) + \frac{\partial_x Z}{\sqrt{|\partial_x Z|}} R_h^{2/3} \partial_x A + A R_h^{2/3} \partial_x \left(\frac{\partial_x Z}{\sqrt{|\partial_x Z|}} \right) = 0 \tag{9.12}$$

which gives:

$$\frac{\partial_x R_h}{R_h} = -\frac{3}{2} \left(\frac{\partial_x F}{F} + \frac{\partial_x A}{A} \right) \tag{9.13}$$

with $F = \frac{\partial_x Z}{\sqrt{|\partial_x Z|}}$. This last expression do not allow to retrieve the bathymetry from the observations since it relates the hydraulic radius R_h to the water surface slope and the cross sectionnal wetted surface. An a-priori hypothesis on the river cross sectionnal geometries along the flow (eg rectangulars) is required to integrate Equation (9.13). Then, the corresponding explicit expression of the bathymetry can be deduced. Since the resulting bathymetry expression is based on the a-priori cross sectionnal shapes, it is not the real bathymetry profile but an effective bathymetry.